LEGIBILITY NOTICE

DIST. CATEGORY UC-63
DOE/JPL-955843/83/8
DRD No. SE5
DRD No. 139

DOE/JPL/955843--83/8

DE83 008871

LARGE-AREA SHEET TASK
ADVANCED DENDRITIC-WEB-GROWTH DEVELOPMENT

C. S. Duncan, R. G. Seidensticker, J. P. McHugh, and
J. Schruben

Annual Report

October 23, 1981 to October 22, 1982
January 18, 1983

Contract No. 955843

The JPL Flat Plate Solar Array Project is sponsored by the U. S. Dept. of Energy and forms part of the Solar Photovoltaic Conversion Program to initiate a major effort toward the development of low-cost solar arrays. This work was performed for the Jet Propulsion Laboratory, California Institute of Technology, by agreement between NASA and DOE.

Westinghouse R&D Center
1310 Beulah Road
Pittsburgh, Pennsylvania 15235

DIST. CATEGORY UC-63
DOE/JPL-955843/83/8
DRD No. SE5
DRD No. 139

LARGE-AREA SHEET TASK
ADVANCED DENDRITIC WEB GROWTH DEVELOPMENT

C. S. Duncan, R. G. Seidensticker, J. P. McHugh, and
J. Schruben

Annual Report

October 23, 1981 to October 22, 1982
January 18, 1983

Contract No. 955843

The JPL Flat Plate Solar Array Project is sponsored by the U. S. Dept. of Energy and forms part of the Solar Photovoltaic Conversion Program to initiate a major effort toward the development of low-cost solar arrays. This work was performed for the Jet Propulsion Laboratory, California Institute of Technology, by agreement between NASA and DOE.

Approved:

R. Mazelsky

R. Mazelsky, Manager
Crystal and Device Technology

Approved:

R. T. Begley, Manager
Solid State, R&D

Westinghouse R&D Center
1310 Beulah Road
Pittsburgh, Pennsylvania 15235

CONTENTS

LIST OF FIGURES

1. SUMMARY

During this reporting period, substantial progress has been made in the reduction of thermally generated stresses in the growing web crystal. These stresses, which if too high cause the ribbon to degenerate, have been reduced by a factor of three, resulting in the demonstrated growth of high-quality web crystals to widths of 5.4 cm. This progress has been brought about chiefly by the application of thermal models to the development of low-stress growth configurations.

A new temperature model was developed which can analyze the thermal effects of much more complex lid and top shield configurations than was possible with the old lumped shield model.

Growth experiments which supplied input data such as actual shield temperature and melt levels were used to verify the modeling results.

Desirable modifications in the melt level-sensing circuitry were made in the new experimental web growth furnace, and this furnace has been used to carry out growth experiments under steady-state conditions.

New growth configurations were tested in long growth runs at Westinghouse AESD which produced wider, lower stress and higher quality web crystals than designs previously used.

2. INTRODUCTION

Silicon dendritic web is a single-crystal silicon ribbon material which provides substantial advantages for low-cost manufacture of solar cells. A significant feature of the process is the growth from a melt of silicon without constraining dies, resulting in an oriented single-crystal ribbon having excellent surface features. In common with other more classical processes such as Czochralski growth, impurity rejection into the melt permits the use of less pure "solar grade" starting material without significantly affecting cell performance. A unique property of the dendritic web process is the growth of long ribbons of controllable width and thickness which not only facilitates automation of subsequent processing into solar cells, but also results in high material utilization since cutting and polishing are not required.

During the previous program (DOE/JPL Contract No. 954654), most of the component elements for the reproducible and steady-state growth of high-quality web crystals were developed and demonstrated. Area throughputs greater than 25 cm^2/min were demonstrated for short periods of time. Melt replenishment for periods of up to 17 hours (a one-day growth cycle) was demonstrated. Thermal models were developed for calculating temperature distributions in the web crystal as a function of configuration parameters.

On the present contract and during the previous reporting period, three broad areas of work were emphasized:

1. The development of thermal stress models in order to understand the detailed parameters which generate buckling stresses. The model can then be used to guide the design of improved low-stress web growth configurations for experimental testing.

2. Experiments to increase our understanding of the effects of various parameters on the web growth process.

3. The construction of an experimental web growth machine which contains in a single unit all the mechanical and electronic features developed previously so that experiments can be carried out under tightly controlled conditions.

Thus, the principal objectives of this work were to expand our knowledge and understanding of both the theoretical and experimental aspects of the web growth process to provide a solid base for substantial improvements in both area throughput and web crystal quality and to develop the tools necessary to carry out this objective.

Although these efforts continued during this reporting period, the emphasis shifted to the application of the tools and knowledge which had been developed in the previous period to the design and experimental verification of low stress web growth configurations.

3. PROGRESS IN WEB GROWTH RESEARCH

3.1 Temperature and Stress Modeling

3.1.1 Introduction

The overall goal of the present program can be described simply as the development of the dendritic web growth process to give greater area throughput of silicon ribbon. One of the most important requirements for satisfying this goal is the reduction of thermally generated stresses in the web, which translates into creating the proper temperature profile along the length of the growing web. Both aspects of area throughput, growth velocity and ribbon width, are dependent directly or indirectly on the temperature distribution in the ribbon.

The growth velocity for any specified crystal thickness is obviously dependent on the temperature profile, since the removal of the latent heat of fusion is directly related to the temperature gradient at the growth front. Although the latent heat can be dissipated through both the liquid and solid, our present concern is primarily with the heat lost through the solid web; the heat lost to the supercooled melt depends on parameters other than those which we will be considering here.

The width of the web crystal depends in a somewhat more indirect fashion on the temperature profile through thermal stresses. These stresses are manifested in two effects: residual stress which is present in the grown material and buckling of the ribbon which occurs during growth itself. Of these two stress effects, the buckling phenomenon represents the most severe limitation to the growth of wide ribbon since both the magnitude of the stress and the stiffness of the ribbon depend strongly on the width of the crystal. Usually a dendritic web crystal is seeded at a narrower width than its desired final dimension and then widens as it grows until either steady state is achieved (width-limited growth) or until something occurs which terminates growth. Buckling is such an event and is manifested by a sudden deformation of the growing ribbon which can, at worst, cause the crystal to pull free of the melt and, at best, make the continued growth of single crystal difficult. Earlier observations of buckled web have shown that material grown immediately prior to the buckling event can be essentially free of residual stress, so that residual stress and buckling can be ascribed to two somewhat different causes. Once buckling has occurred, however, the material usually has a large residual stress, although some recent observations suggest that this may not necessarily be the case. It is important to realize that a zero stress condition is not required to achieve the goals of the dendritic web program. The residual stress observed in ribbon material such as dendritic web is the result of thermal stresses exceeding the material's yield point at some time during growth. When the critical yield stress is exceeded, plastic deformation occurs through the motion or generation of dislocations, resulting in a strained lattice when the material has cooled to room temperature. If the critical yield stress is not exceeded, then an unstrained crystal can be grown. Although the plastic deformation (or, more precisely, the visco-plastic deformation) process is extremely complex, nevertheless extremely perfect dendritic web can be grown even though the thermal stresses were certainly not zero.(1) What is required is to have a thermal stress distribution where the critical yield stress (however defined) is not exceeded.

A similar situation exists with respect to buckling that results from thermal stress. In that case, the critical condition depends on the ribbon width and thickness (stiffness) as well as on the thermal stress itself. As long as the combination of stiffness and stress parameters do not exceed some critical condition, flat ribbon can be grown.

At an earlier point in the development of the dendritic web technique, a purely empirical approach was used to design low-stress growth configurations. Some progress was made but the rate was very slow. Then, computer models were developed to calculate the temperature profile in a growing web and to calculate the stresses generated by these profiles. Most recently, the buckling stability of the web was calculated, i.e., under what conditions of stress and stiffness (width, thickness) would the web switch from growth as a flat ribbon to some curved, buckled shape.(2)

The advantage of this modeling approach is that many weeks of growth experiments, including hardware fabrication as well as actual growth, can be simulated by relatively simple, inexpensive computer calculations. The disadvantage, of course, is that the modeling is only an approximation of reality and the predictions of a model can be trusted only to the extent that the model itself represents the real world. In the present case, the modeling has been shown to give a very good representation of the web growth results as long as the growth geometry can be adequately represented.

The code which calculates the temperature profile could be verified both directly and indirectly. The direct verification was obtained through predictions of the relation between web growth velocity and ribbon thickness. The good correlation between the results calculated for a real growth system and the measured results for that system essentially verified the temperature distribution near the growth front. The adequacy of the results for temperatures further from the growth front was verified by the prediction of buckling behavior which agreed well with the observed web buckling.

Although the temperature calculation code was successful in describing the behavior of relatively simple growth systems -- a crucible with a lid and one or two radiation shields -- it appeared to be the weakest element in the analysis for more complex geometries. Newer growth geometries had more complicated lid designs and three, four, or even more radiation shields. The model was clearly an inadequate representation of such a system. The design of a new temperature calculation code is described later in this report.

Before discussing the current year's results in detail, it is perhaps well to briefly review the philosophy and approach used for the application of the models. A schematic representation of the modeling process is shown in Figure 1. In most instances the modeling sequence begins with the definition of some growth configuration: the shape and temperature of the susceptor lid and the temperature, location, and slot size of the radiation shields above the lid. These parameters may represent a real growth system being studied in the laboratory or they may represent the design of a proposed improved growth system. In the former case, real dimensions and measured temperatures are available; for proposed designs, obviously arbitrary values can be used. However, since the hardware may eventually be fabricated, physically reasonable values are usually chosen. This does not present much of a limitation since a wide range of dimensions and element temperatures are attainable as determined from past experience. The actual choice of dimensions and temperatures for a new proposed design is to some extent empirical in that it is based on analytical and experimental results obtained from previous designs.

Once the web temperature profile has been calculated for a growth configuration, two possible courses of action are possible. First, an iteration on the design could be made on the basis of the temperature characteristics (the (αT)" loop shown in Figure 1). Alternatively, the temperature data can be used as input to the finite element code that calculates thermal stresses in the ribbon, and iteration on the proposed geometry can be done on the basis of the calculated stress distribution. Alternatively, the stress distribution can itself be used as an input to the modeling code that calculates the buckling eigenvalues for the web.

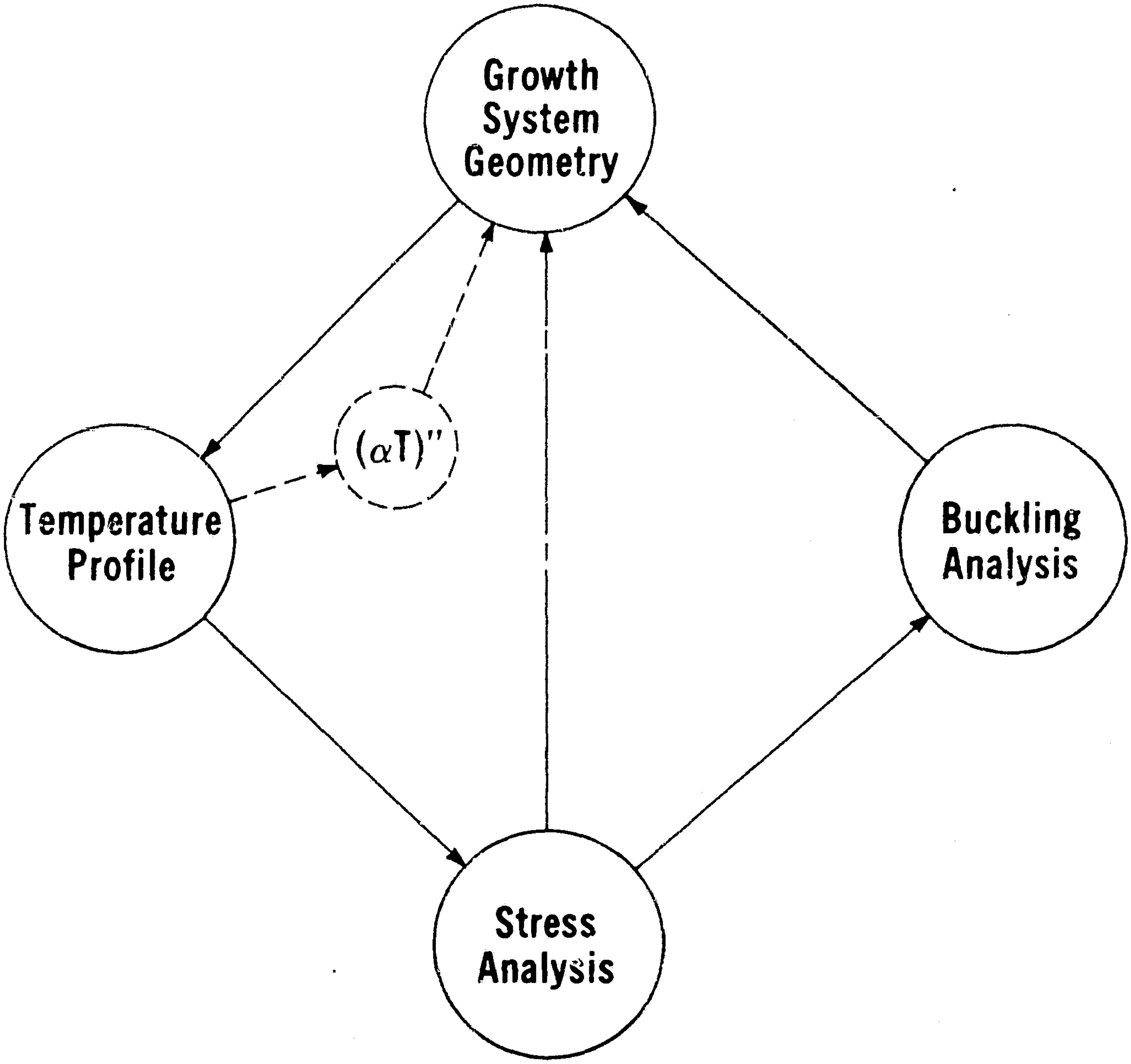

Figure 1 -- Application of computer models.

Not all the temperature profiles used as input to the stress model resulted from analysis of web growth systems. Some temperature distributions were defined from purely mathematical considerations to illustrate isolated features of the "real" profiles. For example, a temperature profile which should produce a constant stress in a long ribbon was used to illustrate the effect of the free boundary at the growth front. The results of several of these "synthetic" profile, runs will be discussed later.

In the following sections, we shall discuss the development of an improved model for calculating web temperature profiles, the results of stress calculations for several "synthetic" temperature profiles, and finally the application of the models to the development of improved growth configurations.

3.1.2 Model Development

3.1.2.1 Introduction

The modeling of the thermal stress and buckling of dendritic web crystals in fact involves three distinct computer codes: 1) a model which calculates the temperature distribution along the growing ribbon; 2) a model which uses the temperature distribution as input and then calculates the thermal stress; and 3) a model which uses the thermal stress distribution as input and then calculates the stability of the ribbon with respect to buckling. With such a sequential type of analysis, it is of obvious importance to have as good as possible a model in the first stage. In fact, the second and third stages of modeling utilize a general, proprietary finite element code, WECAN, which has been shown to be more than sufficiently accurate for our present purposes. The present work concerns improvement of the calculation of the temperature distribution in the web which forms the basis for the subsequent calculations.

The model which calculates the temperature distribution along the growing silicon ribbon has two distinct routines: a routine which calculates the radiative heat exchange between a point on the ribbon and its environment, and a second routine that integrates the heat conduction equation. The problems which occasioned the present work lay not in the integration routine, which had been upgraded earlier, but in the geometrical factors.

For several years, the geometry shown in Figure 2 has been used to evaluate the radiation interchange with the ribbon. This model quite adequately represented the simpler growth configurations used until recently, which had only one or two shields above the lid. Currently, growth configurations with multiple, and occasionally widely spaced, shields are being used, and representation of such a configuration by an isothermal rectangle is suspect. During the reporting period, we have developed a new computer code which allows calculation of the radiative interchange between the web and a number of shields, spacers, etc. so that we have greatly improved the geometric resolution of the model.

As in the previous model, we have neglected other heat transfer mechanisms such as gaseous conduction and convection. Furthermore, we still consider that the absorbance of the silicon ribbon is equal to the emittance, and that the shields, lids, etc. are black bodies so that multiple reflective transfer is neglected. While such refinements might be desired from a theoretical standpoint, the success of the previous modeling suggests that they are second order effects.

3.1.2.2 Review of Radiative Heat Transfer

Consider the radiative transfer between a single shield at Temperature T_i and an element dx of the web at the point x at temperature T(x) (which is to be determined). Figure 3 illustrates the shield subtending an angle from θ_{i1} to θ_{i2} from the normal to the element dx. The radiative flux density from the shield to the point x on the web is

$$\frac{1}{2} \sigma T_i^4 \int_{\theta_{i1}}^{\theta_{i2}} \cos\theta \, d\theta \qquad (1)$$

Dwg. 7768A56

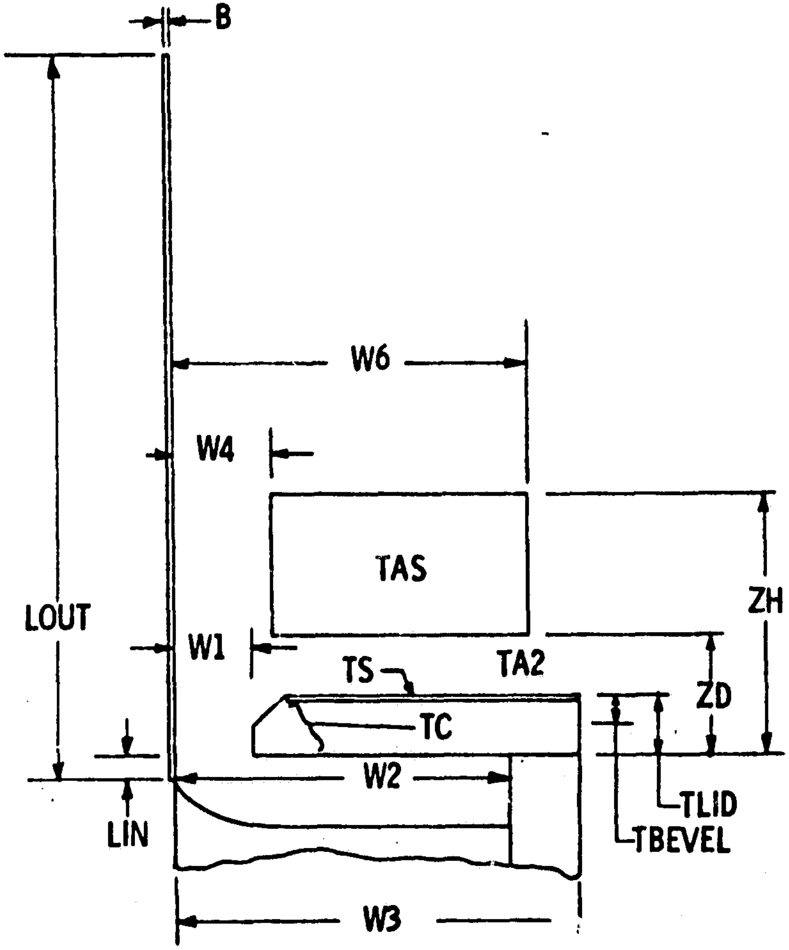

Figure 2. Geometrical and thermal parameters of previous model for calculating temperature profile in the web.

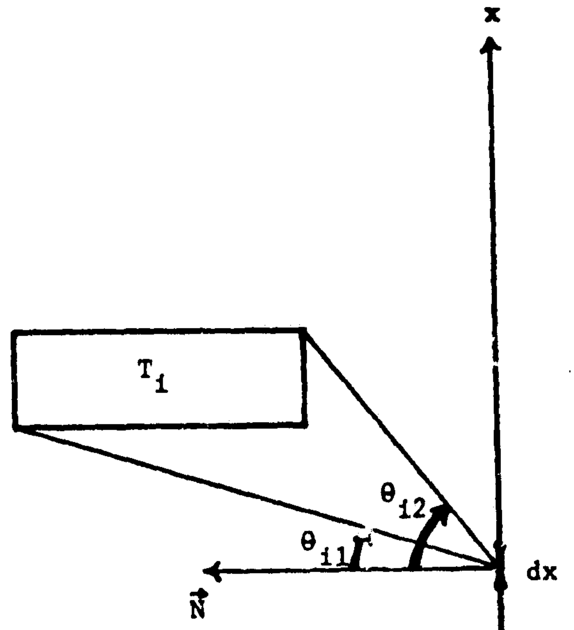

Figure 3. Radiation geometry.

where σ is the Stefan-Boltzman constant. The radiative flux density from the point x to the shield is

$$\frac{1}{2}\,\varepsilon\sigma\ T(x)^4 \int_{\theta_{i1}}^{\theta_{i2}} \cos\theta\ d\theta \tag{2}$$

where ε is the emissivity of silicon web. Since we are assuming the absorbance of the web equals its emittance, the new flux density transferring from x is

$$q = \varepsilon\sigma\ [T(x)^4 - T_i^{\ 4}](\sin\theta_{i2} - \sin\theta_{i1})/2 \tag{3}$$

The net flux density transfer from any number of elements is the sum of terms like the one above. The essential fact is that once the angular limits and temperature of each element are determined, q may be simply evaluated for substitution in the heat transfer Equation 4:

$$\rho Cu \frac{dT}{dx} = \frac{d}{dx}\left(\frac{a}{T}\frac{dT}{dx}\right) - \frac{2q}{t} \tag{4}$$

where ρ = density; C = specific heat; u = pull velocity; a = 318 W/cm, the coefficient of the temperature dependence of thermal conductivity; and t = web thickness. As before, this equation may be integrated to determine the temperature distribution T(x) along the web. We need only evaluate the geometric factors of Equation 3.

3.1.2.3 New Geometry

We examine now the original geometry of Figure 1 to see how it can be systematized for extending its number of elements. A possible systematic arrangement is illustrated in Figure 4; by numbering the ambient regions in sequence with the lid and shields, they may be treated in the same fashion as the other elements. The melt region and the crucible wall are assumed to be at the same temperature and are assigned the number "0". In this case, the ambient region above the top shield would be numbered element 5. The lid is divided into two

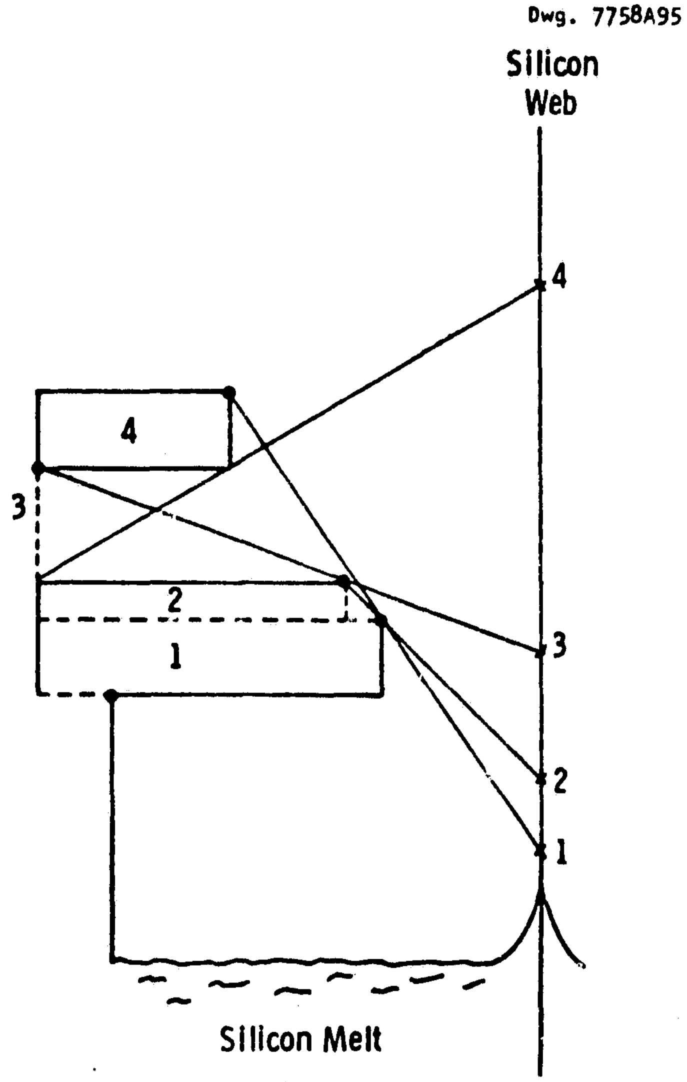

Figure 4. Shading limits for viewing the furnace elements from web.

elements because of the bevel. Since the heat transfer depends only on angular subtense (reflections are neglected), the beveled lid is equivalent to a stepped lid as indicated by the dotted lines. In the previous geometry, the whole lid was isothermal, but now, if desired, different temperatures can be assigned to the top and bottom elements of the lid. In any case, replacing the bevel with a step makes all the elements rectangular in shape. Since the geometries of interest have the back edges of the elements lining up, the ambient spaces can be considered to be comprised of rectangles such as element 3. Thus, the geometry is completely determined by the input of the upper corner of each element indicated by the large, black points.

The four numbered points on the web are the boundaries of regions with different views; for example, for points between 3 and 4, all elements are in view, while above 4, the ambient region 3 is invisible. These points along the x-axis can be systematically determined in the following manner. First, the lower "shade" of each element is found by drawing lines through the inner upper corner of each element below it. The highest intersection of these lines on the x-axis is the lower shade. For example, the point 1 is the lower shade of the 4th element; element 4 is invisible for points on the web below point 1.

After all the lower shades are found (some elements may not have any), then the upper shades are found. The lower inner corner of an element is connected to the lower inner corner of each element above it. The lowest intersection point of each of these lines with the x-axis is the upper shade of the element in question. For example, element 2 does not have an upper shade, while element 3's upper shade is point 4 on the web; element 3 is invisible above point 4 on the web.

After all the upper and lower shades are found, these points are ordered on the x-axis. The region between two such points is assigned a vector, the ith component of which is either one or zero depending on whether or not the ith element is visible to points in this region.

Figure 5 illustrates a possible geometric configuration for the new model. Numerical integration of the heat conduction equation proceeds up the silicon web from the melt surface. By knowing in which region between upper and lower shades the point of integration lies, we know which elements are visible to it. For the point illustrated, elements 0 (the melt), 4, 6, 7, 8, and 15 (ambient) are visible. There is one additional piece of information needed before the integration can proceed: the element opposite the point of integration, element 7 in this case. For the visible elements numbered 7 or less, the lower inner corners are used to limit the viewing angles, while for elements 7 or greater the upper inner corners are used as illustrated. The viewing regions are labeled 1 through 6; these determine the proper coefficient q of the heat conduction equation during integration.

Once the geometrical heat transfer coefficients have been calculated, Equation 4 can be numerically integrated to yield the temperature distribution along the length of the web crystal. A more detailed description of the computer code is presented as an appendix to this report.

3.1.2.4 Verification of the New Model

One of the modeling runs of the J419 configuration, Case 9-11C, was used to verify the new radiation transfer model. The first test was to run the identical configuration, i.e., a lumped shield model as in Figure 2, to verify the operation of the routine which evaluates the shade points, etc. The results were excellent; the new program gave the identical temperature profile as the older program. A second geometry was then evaluated in which both the lid and the shield "block" were beveled. This is a relatively small change in the geometry, but one that could not be accommodated by the older model. It would be expected that the results be similar, but not identical, and that was indeed the case.

Dwg. 7758A96

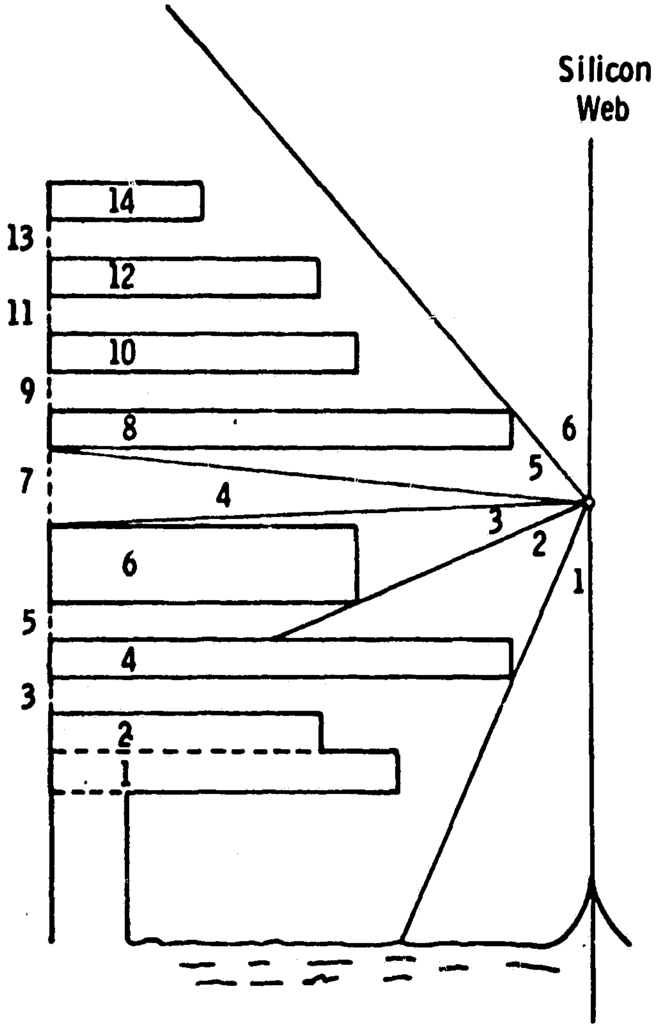

Figure 5. Viewing regions from a point on the web.

Figures 6 and 7 illustrate the two cases.* However, instead of presenting the temperature profiles themselves, the figures show the second derivative of temperature times thermal expansion coefficient, i.e., $(\alpha T)''$. This parameter was chosen because it accentuates the curvature of the temperature which can basically be considered as the cause of thermal stress. Examination of the two figures shows that indeed the two profiles are almost the same, although there are some slight differences due to the more complicated profile.

3.1.3 Operation of the Model

Input options that are available for the model fall into two categories: selection of the operating options of the model such as type of output, number of cases, mode of integration, etc. and, second, the parameters of the configuration being analyzed. A description of the individual data cards as well as a complete listing of the program are included as an appendix to this report.

Output options available for the program fall into three categories: 1) numerical output, 2) graphics output, and 3) punched card output. The first and third output types were previously available, the second output was added when it became apparent that the second derivative of the thermal expansion coefficient times the temperature was a useful parameter for assessing the effect of changes in the shield elements on the thermal stress.

An example of the numerical output is shown in Figure 8. The first column lists the position on the web (the growth front is at 0 cm). The second column gives the calculated temperature. The third and fourth columns are the first and second derivatives of the temperature, and the fifth column is $(\alpha T)''$. All distances are in centimeters and

---

*These figures were generated by a computer plotting routine which has been added to the temperature distribution model. Not only is $(\alpha T)''$ plotted, but also the lid and shield geometry is represented (heavy lines in the figures).

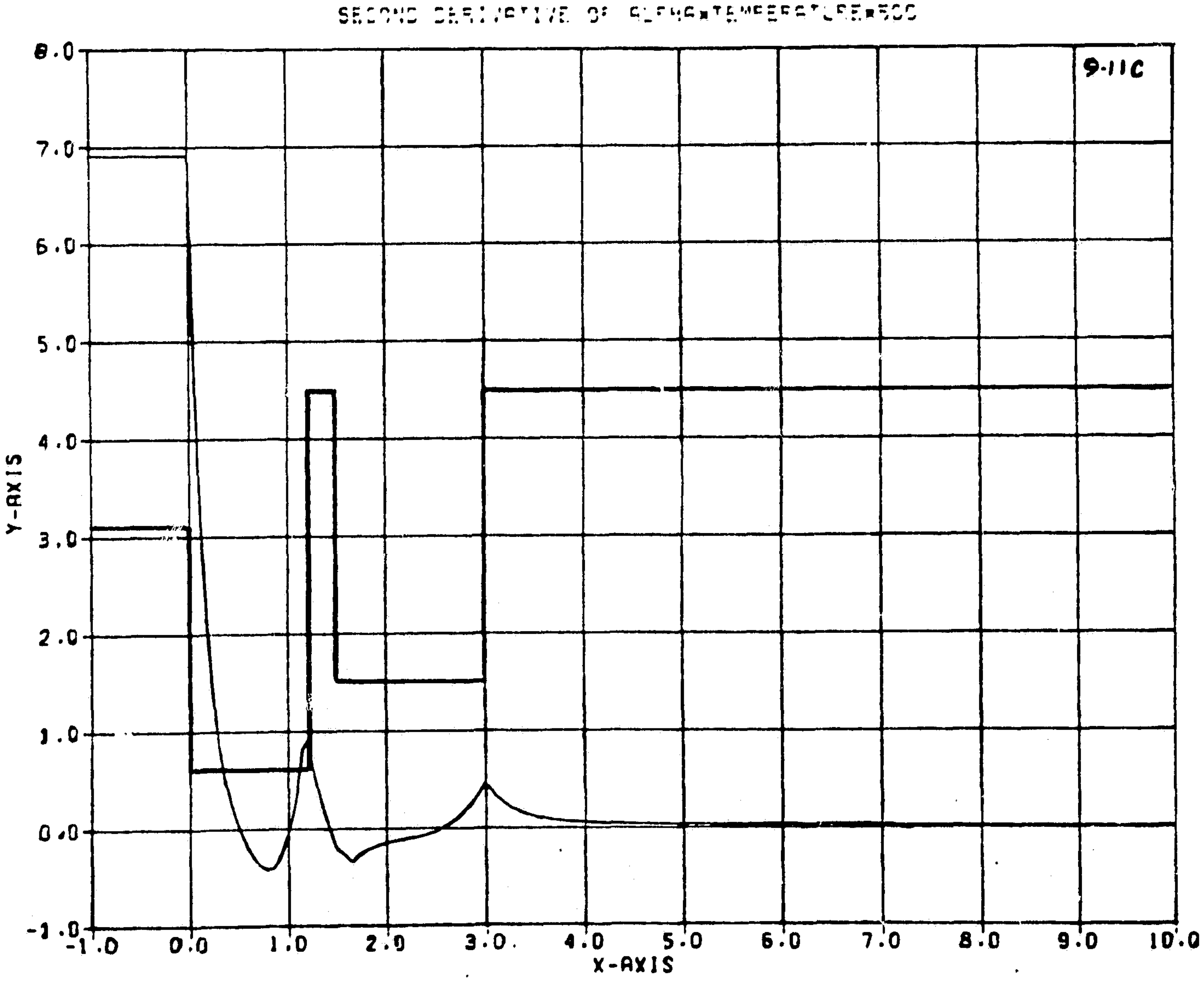

Figure 6. Model geometry and (αT)" for run 9-11C.

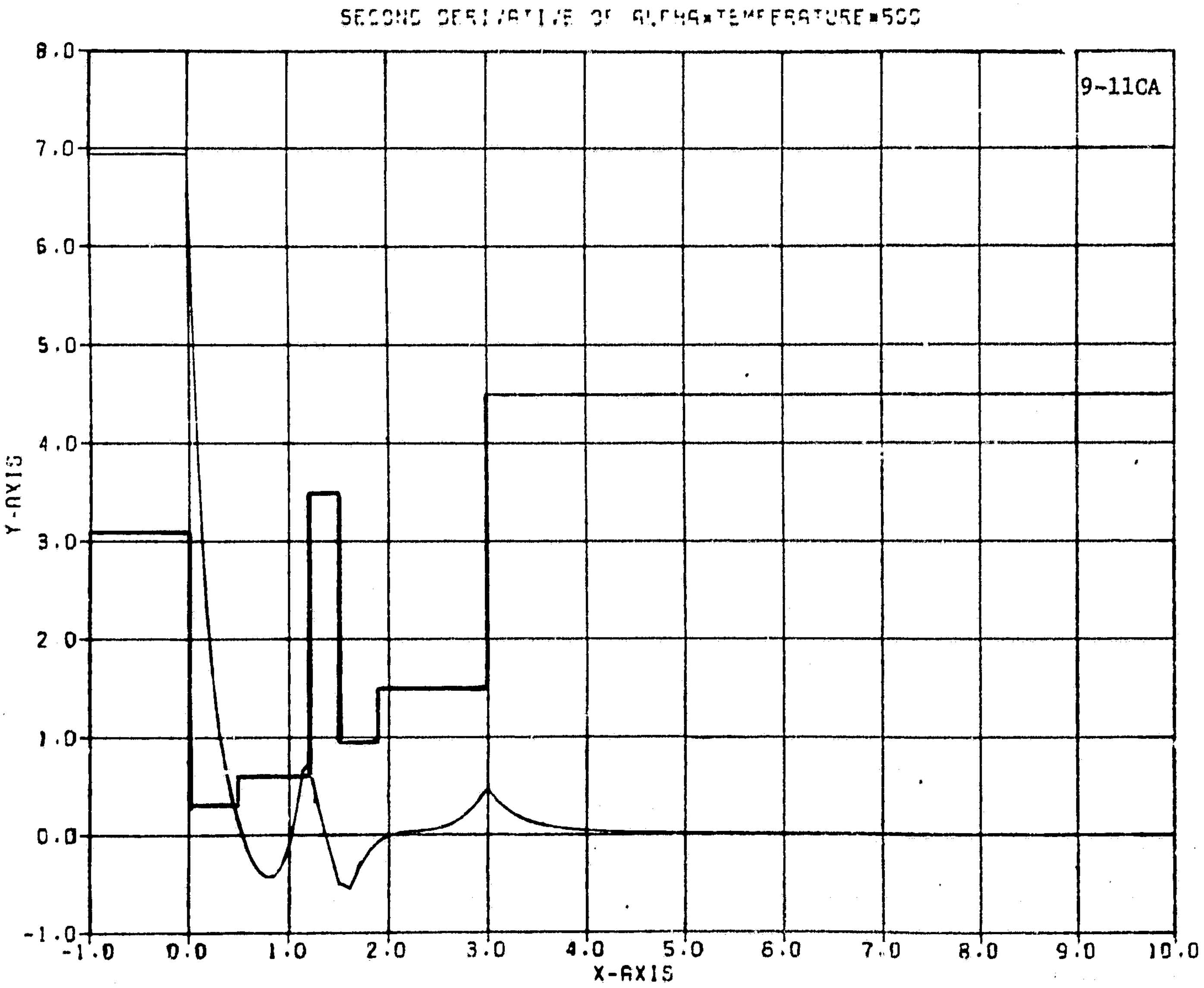

Figure 7. Model geometry and (αT)" for run 9-11CA (beveled elements).

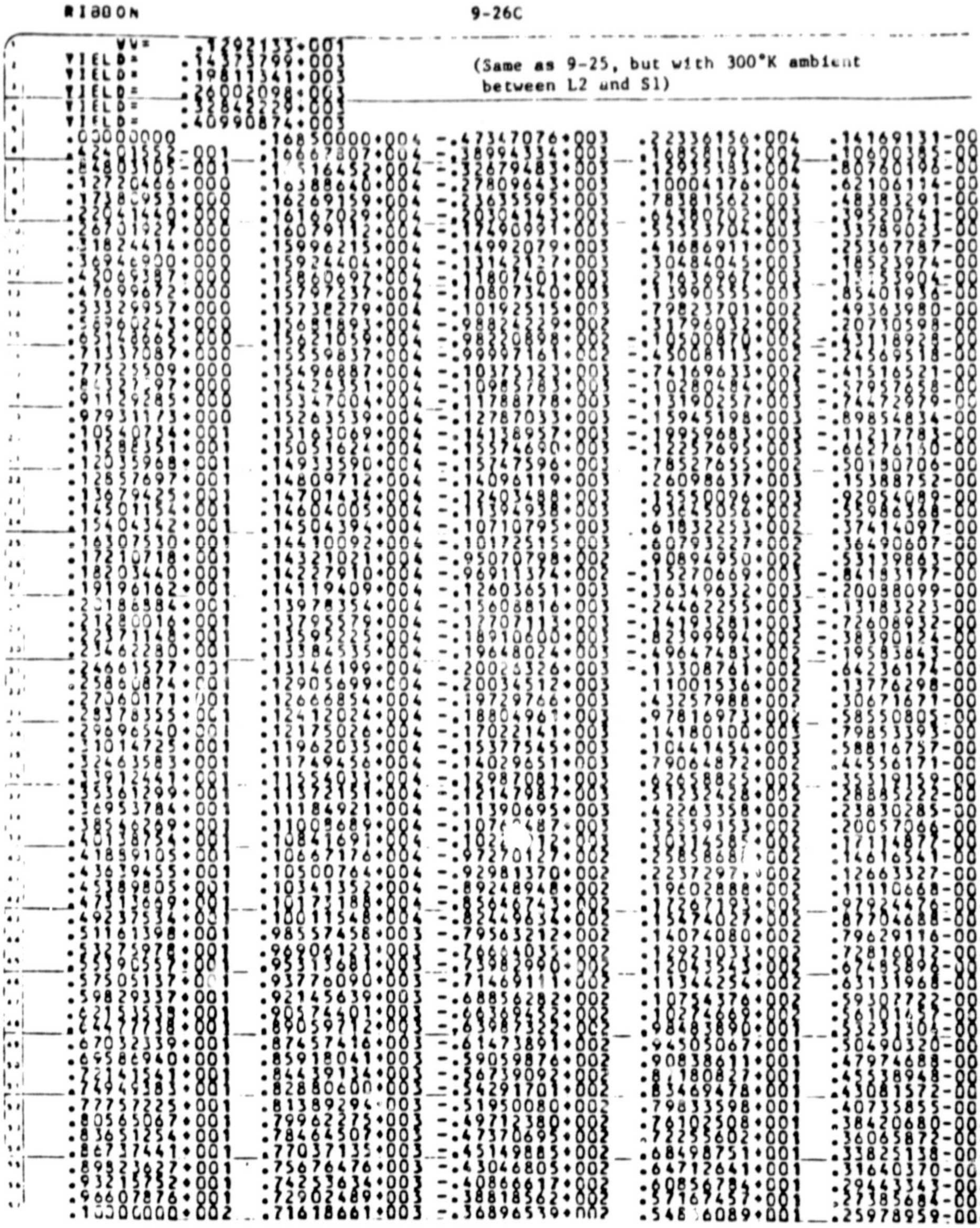

```
RIBBON                                    9-26C
          VV=    .1292133+001
     YIELD=    .14373799+003             (Same as 9-25, but with 300°K ambient
     YIELD=    .19811341+003              between L2 and S1)
     YIELD=    .26002098+003
     YIELD=    .32842229+003
     YIELD=    .40990874+003
 .00000000         .16850000+004  -.47347076+003   .22336156+004   .14169131-001
 .42401552-001     .16667807+004  -.38994334+003   .16858192+004   .10600385-001
 .84803105-001     .16516452+004  -.32679483+003   .12935383+004   .80760196-002
 .12720466+000     .16388640+004  -.27809643+003   .10004176+004   .62106114-002
 .17380953+000     .16269159+004  -.23635595+003   .78381562+003   .48383291-002
 .22041440+000     .16167029+004  -.20304143+003   .64380702+003   .39520741-002
 .26701927+000     .16079112+004  -.17490991+003   .55353704+003   .33789023-002
 .31824414+000     .15996215+004  -.14992079+003   .41686911+003   .25367787-002
 .36946900+000     .15924404+004  -.13142127+003   .30484045+003   .18523974-002
 .42069387+000     .15860697+004  -.11807401+003   .21636967+003   .1[illegible]53904-002
 .47699672+000     .15797237+004  -.10807340+003   .13990555+003   .85401936-003
 .53329957+000     .15738279+004  -.10192515+003   .79823701+002   .49363980-003
 .58960243+000     .15681893+004  -.98824229+002   .31796032+002   .20730598-003
 .65148665+000     .15621059+004  -.98220898+002  -.10500870+002  -.43118928-004
 .71337087+000     .15559837+004  -.99997161+002  -.45008113+002  -.24569518-003
 .77525509+000     .15496887+004  -.10375123+003  -.74169633+002  -.41516521-003
 .84327397+000     .15424351+004  -.10985783+003  -.10280484+003  -.57957658-003
 .91129285+000     .15347004+004  -.11788778+003  -.13190257+003  -.74472979-003
 .97931173+000     .15263539+004  -.12787033+003  -.15945198+003  -.89854834-003
 .10540734+001     .15163069+004  -.14138957+003  -.19959683+003  -.11217783-002
 .11288351+001     .15051624+004  -.15574690+003  -.12257695+003  -.66276130-003
 .12035968+001     .14933590+004  -.15747596+003   .78527655+002   .50180706-003
 .12857697+001     .14809712+004  -.14096119+003   .26098637+003   .15388752-002
 .13679425+001     .14701434+004  -.12403488+003   .15550096+003   .92054089-003
 .14501154+001     .14604005+004  -.11394938+003   .93645056+002   .55986368-003
 .15404342+001     .14504394+004  -.10710795+003   .61832253+002   .37414097-003
 .16307530+001     .14410092+004  -.10172515+003   .60793227+002   .36490607-003
 .17210718+001     .14321021+004  -.95070798+002   .90894950+002   .53139863-003
 .18203440+001     .14227910+004  -.96911374+002  -.15270669+003  -.84183177-003
 .19196162+001     .14119409+004  -.12603651+003  -.36349632+003  -.20088099-002
 .20188884+001     .13978354+004  -.15608816+003  -.24462255+003  -.13183223-002
 .21280016+001     .13795579+004  -.17707113+003  -.14193281+003  -.72608932-003
 .22371148+001     .13595225+004  -.18910600+003  -.82399994+002  -.38390124-003
 .23462280+001     .13384535+004  -.19648024+003  -.49647483+002  -.19583843-003
 .24661577+001     .13146199+004  -.20023326+003  -.13308761+002   .64236174-005
 .25860874+001     .12905699+004  -.20034512+003   .11001536+002   .13776298-003
 .27060171+001     .12666854+004  -.19729766+003   .43257988+002   .30671671-003
 .28378355+001     .12412024+004  -.18804961+003   .97816973+002   .58550805-003
 .29696540+001     .12175026+004  -.17022141+003   .14180100+003   .79853393-003
 .31014725+001     .11962035+004  -.15377545+003   .10441454+003   .58816757-003
 .32463583+001     .11749456+004  -.14029651+003   .79064872+002   .44556171-003
 .33912441+001     .11556033+004  -.12987081+003   .62658825+002   .35319159-003
 .35361299+001     .11372151+004  -.12147987+003   .51232428+002   .28885222-003
 .36953784+001     .11184921+004  -.11390695+003   .42263358+002   .23830285-003
 .38546269+001     .11009689+004  -.1076[illegible]487+003   .35559153+002   .20057066-003
 .40138754+001     .10841691+004  -.102[illegible]12+003   .30314585+002   .17114877-003
 .41859105+001     .10667176+004  -.97270127+002   .2585868[illegible]+002   .14616541-003
 .43639455+001     .10500764+004  -.92981370+002   .2237297[illegible]+002   .12663327-003
 .45389805+001     .10341352+004  -.89248948+002   .19602888+002   .11110668-003
 .47313669+001     .10173188+004  -.85646743+002   .17267193+002   .97924476-004
 .49237534+001     .10011548+004  -.82449634+002   .15474027+002   .87704688-004
 .51161398+001     .98557458+003  -.79563212+002   .14074080+002   .79629116-004
 .53275978+001     .96906123+003  -.76664035+002   .12921033+002   .72816012-004
 .55390557+001     .95313681+003  -.73982990+002   .12043543+002   .67485896-004
 .57505137+001     .93776090+003  -.71469111+002   .11344254+002   .63131968-004
 .59829337+001     .92145639+003  -.68856282+002   .10754376+002   .59307722-004
 .62153538+001     .90574601+003  -.66369452+002   .10274669+002   .56101457-004
 .64477738+001     .89059712+003  -.63987325+002   .98483890+001   .53231304-004
 .67032339+001     .87457416+003  -.61473891+002   .94505067+001   .50490320-004
 .69586940+001     .85918041+003  -.59059876+002   .90838611+001   .47974688-004
 .72141541+001     .84439134+003  -.56739092+002   .8[illegible]180827+001   .45538948-004
 .74949383+001     .82880600+003  -.54291701+002   .83469478+001   .43081572-004
 .77757225+001     .81389294+003  -.51950080+002   .79833598+001   .40735855-004
 .80565067+001     .79962275+003  -.49712380+002   .76102508+001   .38420680-004
 .83651254+001     .78464507+003  -.47370695+002   .72255602+001   .36065872-004
 .86737441+001     .77037135+003  -.45149885+002   .68498751+001   .33825138-004
 .89823627+001     .75676476+003  -.43046805+002   .64712641+001   .31640370-004
 .93215752+001     .74253634+003  -.40866617+002   .60856784+001   .29443343-004
 .96607876+001     .72902489+003  -.38818562+002   .57167457+001   .27385684-004
 .10000000+002     .71618661+003  -.36896539+002   .548[illegible]6089+001   .25978959-004
```

Figure 8. Example of numerical output from new web temperature computer code.

temperatures are in ^{o}K. In addition to this data, two other sets of data are listed at the top of the printout. The first, labeled VV, is the partial growth velocity of the web resulting from the heat lost from the web crystal itself. This differs from the total growth velocity which is observed in experiments by a contribution which results from some of the latent heat being dissipated to the supercooled melt.(4) An estimate of this total growth velocity is included as one of the input parameters to the model.

The second set of data included is an estimate of the critical yield stress for the web corresponding to the first five temperature points. The yield stress is simply an estimate based on an empirical equation from the work of Graham et al.(2,5)

$$\sigma_{YP} = 2.57 \times 10^{-11} \exp(49459/T) \text{ Mdyn/cm}^2 \qquad (5)$$

These critical-yield stress values can be used later when actual stress distributions are generated by the finite element WECAN calculations. Although the viscoelastic phenomena responsible for the observed residual stress in the crystals is extremely complex, these data provide a first estimate of possible effects. The first four columns in the balance of the numerical data are more or less self-explanatory in being the position, the temperature, and its first two derivatives. The last column, $(\alpha T)''$, is of importance since it is basically the generating function for the thermal stress. Although the relationship between $(\alpha T)''$ and stress is not straightforward near the interface where the free boundary exerts a strong influence, it is relatively simple elsewhere where the Boley and Weiner approximation(6) applies:

$$\sigma_x = \frac{E}{6} (3y^2 - w^2) (\alpha T)'' \qquad (6)$$

where E is Young's modulus and w is the half width of the ribbon. Through the relationship of T" with the heat loss from the ribbon, it is possible to correlate the behavior of this parameter with changes in the geometry of the lids and shields.

Realization of the usefulness of the $(\alpha T)''$ parameter led to the addition of a graphics output capability to the code. Since the end application was to compare the $(\alpha T)''$ function with the geometry being analyzed, the graphics output presents both a representation of the lid and shields and the concomitant $(\alpha T)''$ curve. If the geometry does not change (lid, shield, and interface position), then up to three different $(\alpha T)''$ curves can be represented on the same plot. A representative output is shown in Figures 6 and 7; the plot of the lid and shields has been accented for the sake of emphasis.

The final output option from the program is a set of punched cards giving the nodal temperatures for use with the WECAN stress calculations. In this option, there are several sub-options depending on whether a two-dimensional stress calculation or a three-dimensional buckling calculation is to be done. Further, in the two-dimensional calculation, there is a choice as to whether quadratic or cubic elements are employed. Also, some choice is available as to some of the geometric features of the finite element grid.

Thus, the program to calculate the web temperature distribution has a great deal of flexibility in both the lid and shield configuration which can be analyzed, and in the options for presenting the results of its calculations. The flexibility of both the input and output greatly enhance the ability of the program to assist in the analysis and design of dendritic web growth configurations.

3.1.4 Stress Model Development

Although most of the development of the models themselves was concerned with the temperature code, some investigations of the stress and buckling models were also made. The concern was not so much with the computer code itself, which is well validated, as with the application of the proper boundary conditions, especially with the buckling calculations. The question gained importance as wider and wider crystals were being grown and the growth systems analyzed. Calculations with "synthetic" temperature profiles suggest that the "end effect" due to the free boundary at the end of the web extends longitudinally for a distance about equal to the full width of the ribbon. Although this should be a good approximation to reality for the melt end of the crystal, it could lead to an underestimate of buckling when also used at the "ribbon end" of the finite element mesh, especially when the crystal width approached 5 cm and the mesh length was only 10 cm. A longer mesh could of course be used, but to make much difference the increased length would be significant and would lead to increased calculation time. A simple change in the boundary conditions could possibly accomplish the same end and would not affect computer usage.

In calculating the stresses resulting from a given temperature profile, appropriate temperatures are assigned to the nodes of a mesh of elements. In addition, boundary conditions must be specified for the edges of the mesh. At the boundary representing the growth front, the appropriate condition is the free boundary $\sigma_x = 0$, i.e., no longitudinal stress. On the free edge of the strip, the condition is $\sigma_y = 0$, i.e., no lateral stress. The center of the strip is a line of symmetry so that the condition there is zero y displacement $u_y = 0$. The uncertainty arises at the end of the mesh which "connects" to the rest of the ribbon; previous practice has been to consider this to be another traction-free boundary with $\sigma_x = 0$ as at the melt end of the mesh. A possible alternative condition would be to require that all x-displacements be the same at the boundary, i.e., $u_x = \text{const}$.

The two possibilities were tested by calculating the buckling eigenvalues for a model of the J460 configuration, which was known to be capable of growing undeformed crystals over 40 mm wide at thicknesses of 150 μm or less. A 39.5 mm width was assumed for the model (37 mm web with 1.25 mm dendrites on each edge). The free-boundary condition predicted a critical width of 39.9 mm for buckling, which is slightly narrower than actually observed, while the constant displacement condition predicted a critical width of 35.1 mm. Obviously, the free boundary condition is much closer to observation and in fact is slightly conservative. Examination of the stress distributions showed that the "free-boundary" condition was probably much closer to the probable actual stress than the "constant-displacement" condition, in agreement with the buckling predictions. It would appear therefore, that our present application of the stress and buckling codes is adequate for evaluating material up to about 45 or 50 mm; but when wider growth is predicted, then the finite element mesh must be extended to preserve good agreement between the model and reality.

Another topic which was investigated was the relation between ribbon width and stress magnitude. Usually a 27 mm crystal is assumed for calculation of stress when evaluating a temperature profile with a two-dimensional stress model. This width has been appropriate to real crystal dimensions and by holding the width constant, comparison of various temperature profiles was facilitated. With the growth of wider and wider crystals, however, we wanted to know how stress might vary with width.

A temperature profile was calculated for one of the J460 type configurations and two-dimensional stress calculations were made for 17 mm, 27 mm, and 39.5 mm models. Surprisingly, the y-stress distribution near the growth front varied only slightly with width, especially for the two wider models. The x-stresses further from the growth front varied more strongly with width, but the relationship was more nearly $W^{1.3}$ than W^2 as expected from simple theory.

These results are consistent with some observations of web growth in the laboratory. When a poor growth configuration is used, even narrow crystals will have relatively large residual stress, which would evidently be expected if the y-stress near the growth front is the causitive factor.

3.1.5 Synthetic Temperature Profiles

Previous studies of thermal stress and buckling have used mathematical models to evaluate the performance of real, or at least proposed, lid and shield configurations. This type of analysis has been continued during the present period but, in addition, stresses were computed for several temperature distributions which were synthesized purely on the basis of their mathematical properties. These "synthetic" temperature profiles were evaluated to illustrate the requirements of a low-stress profile.

Boley and Wiener$^{(6)}$ have published an often-cited series solution for the stress components in a uniform ribbon having a temperature distribution varying only with x (the coordinate along the length of the ribbon). The first term of their result for σ_{xx} is

$$\sigma_{xx} = \frac{\alpha E w^2}{6} \left(3 - \frac{y^2}{w^2}\right) T'' \qquad [6a]$$

where α is the thermal expansivity (assumed to be constant), E is Young's modulus (also constant), w is the half width of the ribbon, and y is the width coordinate. The prediction of equation 6a, that $\sigma_{xx} = 0$ if $T'' = 0$, does not hold if the thermoelastic properties (α or E) vary with temperature; for our calculations we assume that E is constant but allow α to depend on temperature. The condition for zero stress is then $(\alpha T)'' = 0$, and for constant stress, Equation 6a becomes

$$(\alpha T)'' = 6\sigma_{xx}/E(3w^2 - y^2) \qquad [6b]$$

By assuming an analytic form for $\alpha(T)$, e.g., $\alpha = \alpha_0 + \alpha_1 T$, Equation 6b can be solved to identify temperature distributions giving constant stress in the ribbon. A series of such temperature distributions is shown in Figure 9, where the parameter labeling the curves is the difference in stress between the ribbon center and ribbon edge.

Curve 730152-A

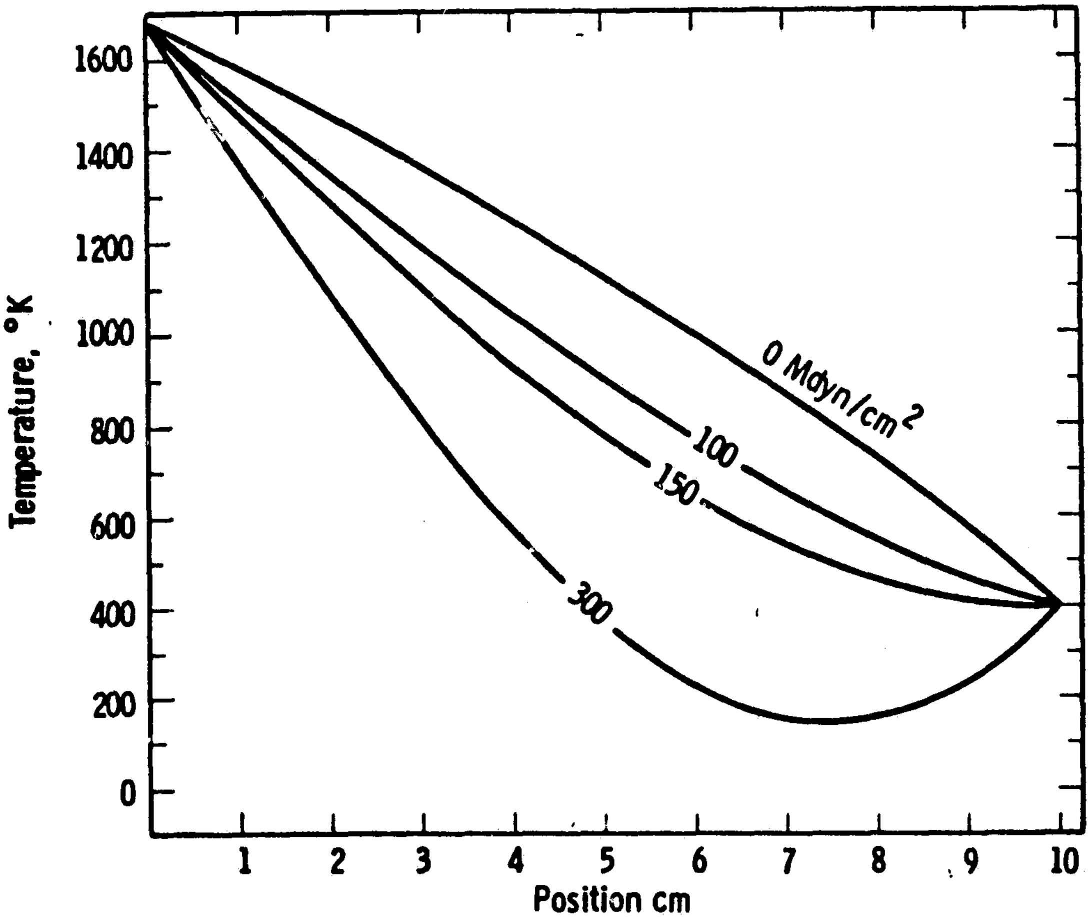

Figure 9. Constant stress temperature profiles.

The series solution from which Equation 6a was derived only applies when end effects are negligible and when T" (or(αT)") is not changing rapidly. Both of these conditions are violated near the growth front of the dendritic web. Since essentially zero tension is applied to the growing interface, the growth front is a traction-free boundary. Further, because of the rapidly changing high temperature of the ribbon in this region, T" also changes rapidly. In order to develop at least a semi-quantitative understanding of the effect of these two conditions on the thermal stresses, two "synthetic" temperature profiles were used as input data for the WECAN stress calculations.

To illustrate the effect of the traction-free boundary, a temperature profile was used that would generate a constant stress according to Equation 2. The traction-free boundary condition was intrinsic to the WECAN analysis used for the calculation.

The modeling of this profile was actually run twice. The first run gave results which were very close to the predictions of Equation 6b but differed in some small details. It was then realized that the mesh used in the stress computation included elements which represented the additional stiffening due to the bounding dendrites. The same temperature profile was then rerun using a mesh representing a uniform ribbon without dendrites, and the results were in exact agreement with the theory.

The result is shown in Figure 10, which depicts $\Delta\sigma_{xx}$ along the ribbon. This stress parameter was chosen since it reduces the "grain" inherent in the finite element calculations. From simple inspection of the curve, it can be seen that the end effect of the free boundary extends for a distance approximately equal to the ribbon width (2.7 cm in this calculation). Although the fit is not exact, the effect of the boundary seems to be approximately a complementary Gaussian with a characteristic length equal to the ribbon width. This result shows that the details of the (αT)" curve near the growth front are mitigated to a large extent by the end effect. This may be of importance in future

Curve 739388-A

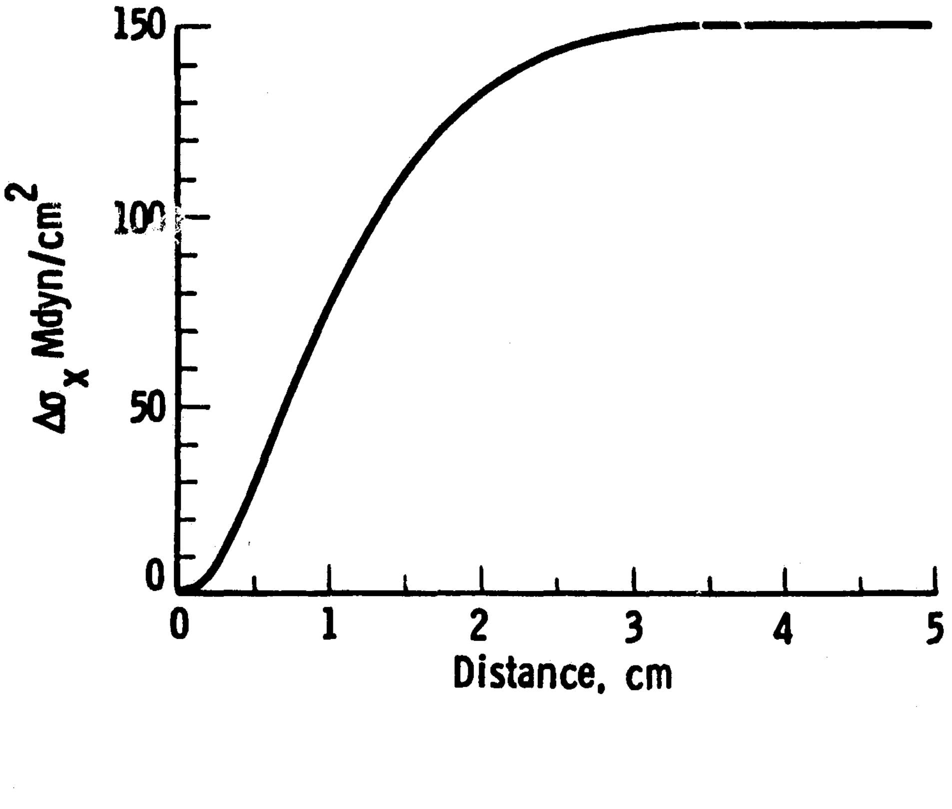

Figure 10. End effect region of constant stress profile.

lid/shield design efforts in that the design itself may be separable into two regions: one near the growth front and one further up the crystal.

The second synthetic temperature profile was intended to show how stresses caused by changes in $(\alpha T)''$ affect adjacent regions of the crystal. The temperature profile used for the analysis was composed of two zero stress segments with the transition at the midpoint of the finite element mesh. Thus, $(\alpha T)'' = 0$ everywhere, but all the higher derivatives were essentially infinite at the midpoint to give an effective delta function for thermal stress generation.

The results of the WECAN calculations are shown in Figure 11; 11a is the temperature distribution used as input for the WECAN analysis, and 11b is the resulting σ_x and σ_y. The effect of discontinuity in the curvature of the profile obviously spreads over a significant region of the crystal. Again, the σ_x distribution is approximately a Gaussian with a characteristic length of the ribbon half-width.

The importance of the results in this run lie in understanding the interaction of different regions of the $(\alpha T)''$ curve. In the previous analysis of web growth configurations, it was obvious that there was a connection between the stress components and the $(\alpha T)''$ values, but it was certainly not as simple as implied by Equation 6a. The present result indicates that an averaging (or perhaps a convolution) analysis is more appropriate but further gives some indication as to the magnitude of the characteristic distance.

The third synthetic temperature profile assumed an exponential decay of the $(\alpha T)''$ profile from its value near the interface. This particular function was chosen since it is a reasonable approximation to the behavior observed in models of any realistic lid/shield configurations, although in those cases the exponential behavior is found only in the first 5 mm or so. The stress distribution from the synthetic temperature case was in reasonable quantitative agreement with

Curve 739389-A

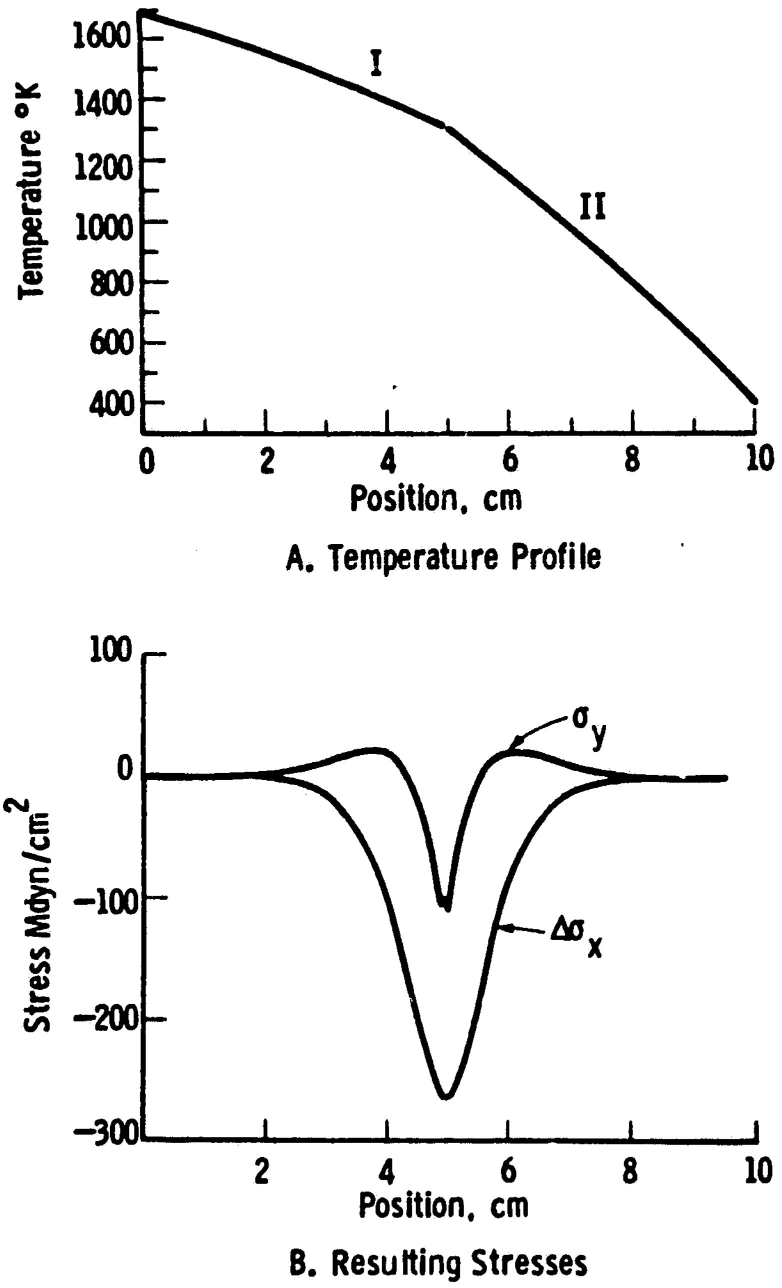

Figure 11. Stresses generated by abruptly changing zero stress temperature profiles.

the stress distributions in the interface region of the more realistic cases, although of course the more distant features were quite different. In both the synthetic and realistic cases, the actual x-stress magnitude near the boundary was far smaller than might be anticipated, in agreement with the boundary effect of the constant stress case. These results indicate that the initial $(\alpha T)''$ peak is responsible for much of the thermal stress behavior at the interface, but also that there are other factors such as the free-boundary effect which must be considered. It is also not yet clear to what effect the peak height and the characteristic decay length of the exponential are involved in the stress generation. These factors need some additional runs to clarify the behavior. The final results should be applicable to the design of lid configurations for faster growth with lower residual stress.

3.1.6 Development of New Configurations

Although the model development and the studies of synthetic temperature profiles described in the preceding sections have some intrinsic importance, their primary purpose is to provide the tools and guidance for the development of improved dendritic web growth systems. During the reporting period, two principal designs were developed: the J419 and J460 series of growth hardware. Each proved to be a distinct improvement over preceding designs and each has gone through a series of design modifications for use in melt replenished, steady-state growth.

J419. As indicated by the design designation (run J419 was the first experimental evaluation of the configuration), J419 was the first of the two designs. Development of the design followed from the hypothesis that buckling in dendritic web growth was related to a large peak in the x-stress distribution which occurred several centimeters above the growth front. This peak in the stress distribution in turn appeared to be related to a small maximum in the $(\alpha T)''$ distribution calculated by the temperature model. These features are illustrated in Figures 12 and 13 for a temperature profile representative of the J98M3 configuration, one of the best prior configurations.(7) The maximum $\Delta\sigma_x$ [$= \sigma_x$ (center - σ_x(edge)] is 615 Mdyn/cm^2 and the associated $(\alpha T)''$ is 1.2×10^{-3} cm^{-2}. The goal of the development work was to reduce these parameters.

The design of a new configuration is based on prior experience, both analytical and experimental, by observing the relationship between growth performance and the characteristics of the configurations as calculated from the models. Experience with various modeling runs, both for real growth configurations and with the "synthetic" temperature profiles, suggested that some additional localized heating was needed near the growth front while maintaining the loss to furnace ambient. In addition, losses further along the crystal should be reduced to lower the large x-stress peak. These design requirements translated into a relatively thick, hot lid with a relatively tall shield stack having shield slots of increasing width.

The resulting configuration is shown in Figure 14. The lid itself is thicker -- 0.5 inch instead of the .38 inch or .25 inch lid used in previous configurations. Surmounting the lid are four shields with slot openings arranged so that the web at the growth front has a 25.6° clear view of the cold furnace interior. This configuration was analyzed for thermal stresses using lid and shield temperatures deduced from measurements on other configurations. The temperature calculations indicated a "far peak" value for $(\alpha T)''$ of about 8.1×10^{-4} cm^{-2} and the $\Delta\sigma_x$ profile, shown in Figure 15, shows that the accompanying stress has been reduced to about 360 Mdyn/cm^2.

On the basis of the calculated thermal stresses, a full buckling analysis was performed on the model. The results indicated that a 150 μm thick web crystal would not buckle at widths narrower than 38 mm. This was a substantial improvement over previous designs and the decision was made to fabricate a set of lids and shields that would give a real growth system representing the design analyzed with the models.

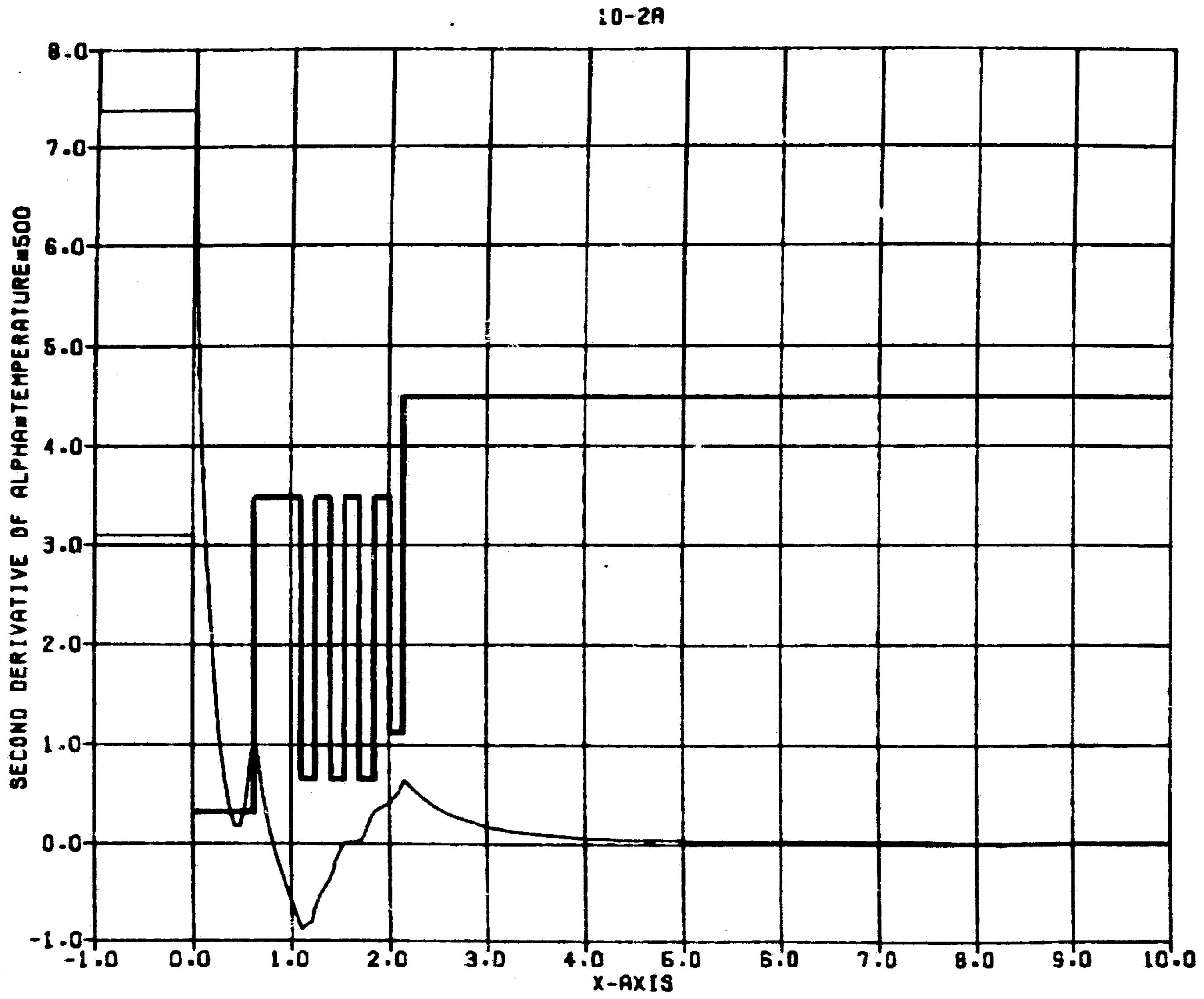

Figure 12. Temperature model of J98M3 configuration.

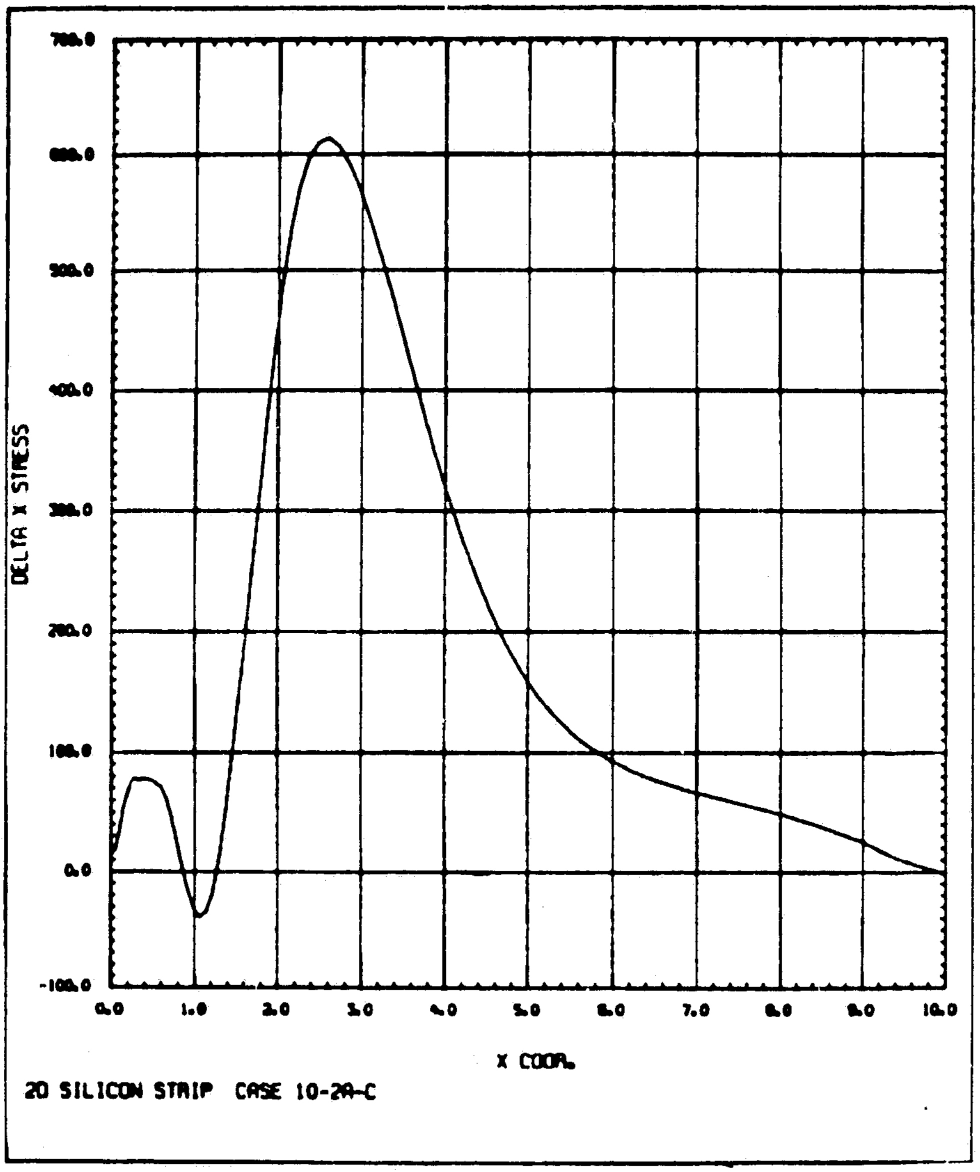

Figure 13. Delta x-stress for J98M3 configuration.

Dwg. 7767A15

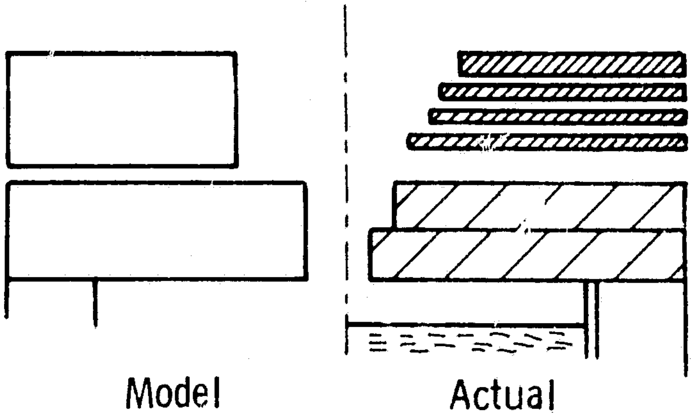

Figure 14. J419 configuration.

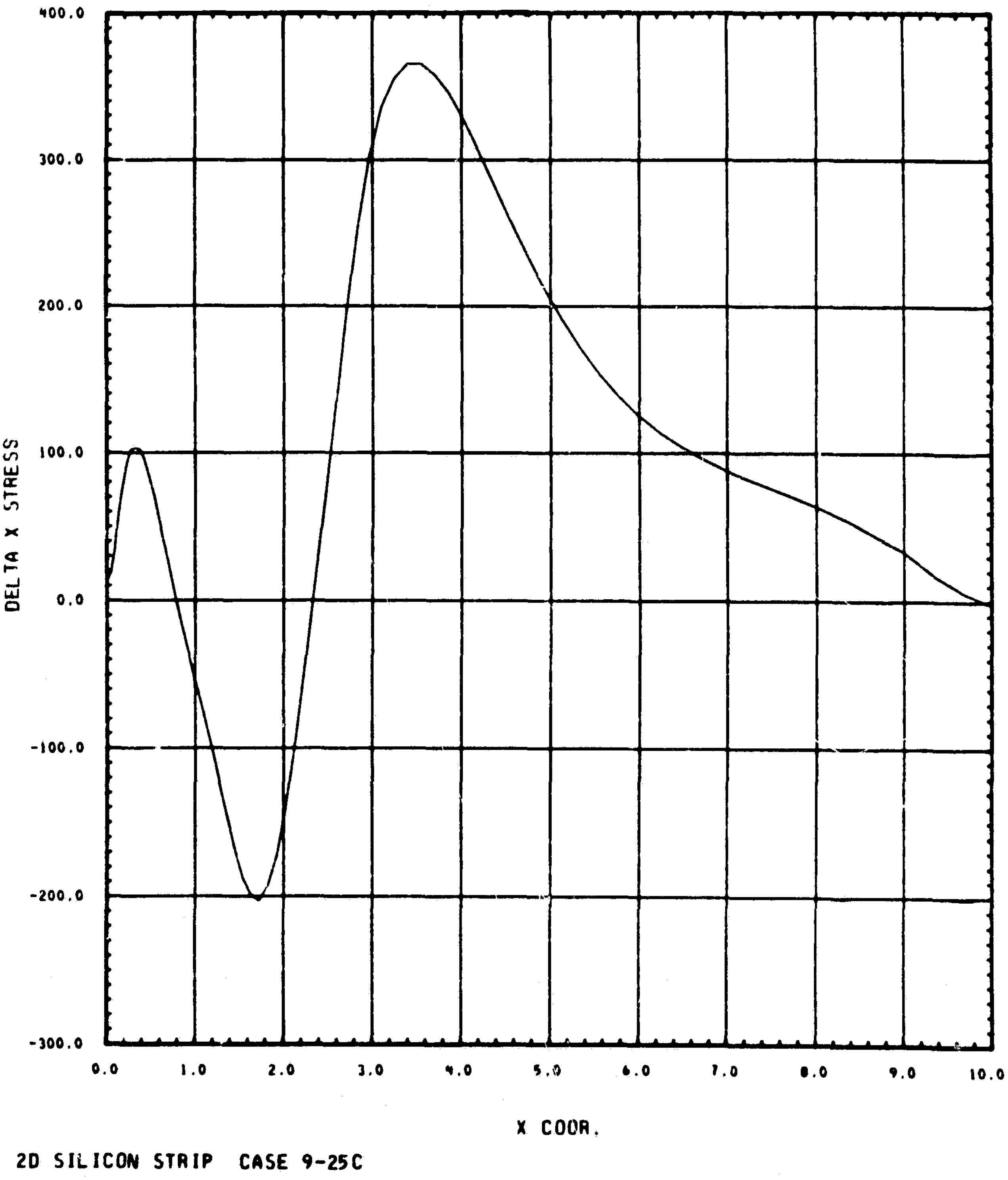

Figure 15. Delta x-stress for J419 configuration.

The initial run of the configuration included thermocouples in the lid, bottom shield, and top shield. The measured temperatures were consistent with the temperatures assumed for the stress and buckling. More important, however, was the result that in the initial run an unbuckled crystal was grown to a width of 35 mm, although the thickness was only 125 μm. In subsequent runs, thicker web (190 μm) was grown to a width of 44 mm without buckling and to 49.9 mm with only slight deformation. These width and thickness values are in almost perfect agreement with the buckling predictions.

J460. Although the J419 was a marked improvement over previous configurations, it was felt that further improvement could be made following the same design philosophy. A thicker lid would hopefully improve the temperature distribution near the growth front to give low residual stress, while an even higher shield stack would reduce the stress peak away from the interface to reduce the "buckling" stress. In choosing a geometry to model, a recessed lid of the J352 type(7) was used for L1 with a solid lid for L2; the recessed lid would minimize gas conductivity effects while not changing the radiative heat transfer. Thus, a real system would more closely approach the assumptions in the modeling.

The results of the temperature profile calculations are shown as a $(\alpha T)''$ plot in Figure 16. The recessed lid geometry is apparent from the geometry plot (accented) which is part of the figure. In this calculation, the $(\alpha T)''$ maximum has been reduced to 2.3×10^{-4} cm^{-2} and the resulting $\Delta\sigma_x$ is only 195 Mdyn/cm^2 as seen in Figure 17. The growth experience with this configuration confirms the low-stress aspects predicted by the models.

In summary, the use of temperature and stress models to identify the sources of thermal stress in dendritic web growth systems has led to marked improvement in the growth hardware. Very early configurations had stress peaks as large as 1200 to 1500 Mdyn/cm^2; the J98M3 configuration had a peak of about 615 Mdyn/cm^2; the J419 peak was about

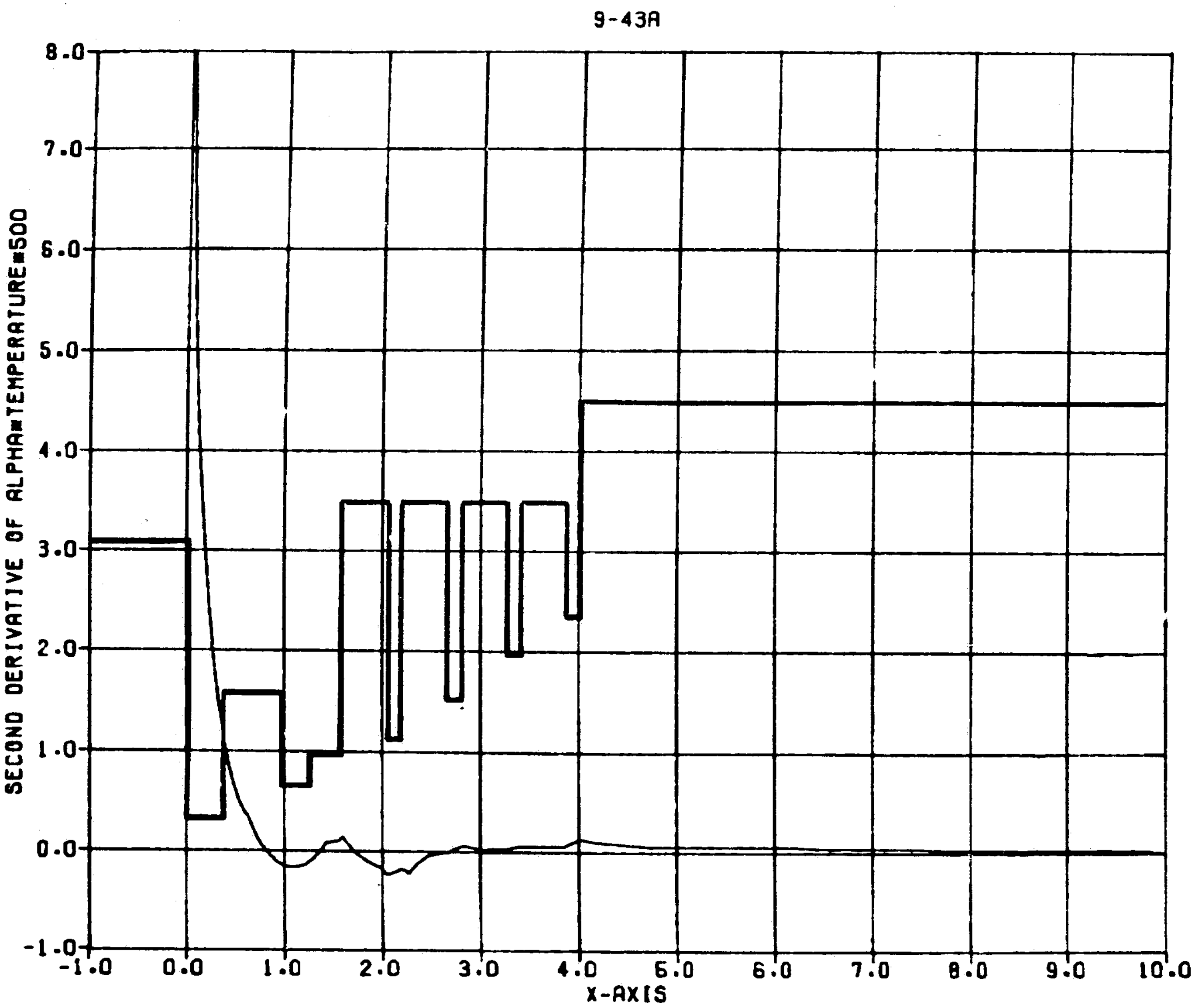

Figure 16. Temperature profile results for J460 configuration.

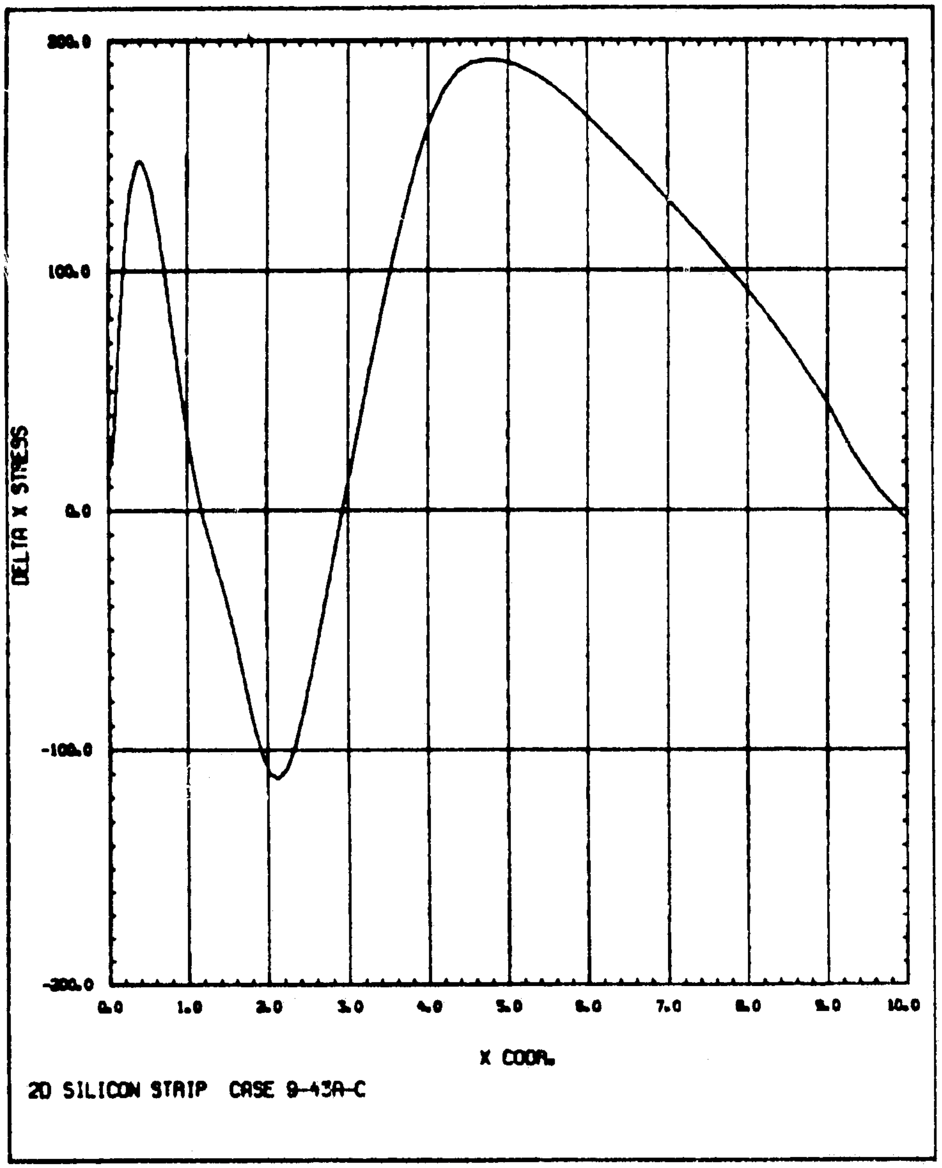

Figure 17. Delta x-stress distribution for J460 configuration.

350 Mdyn/cm^2, and in the J460 configuration the peak was only 195 Mdyn/cm^2. With each reduction in peak height, wider web was grown. Even further improvement will be possible.

3.2 Operation of the New Experimental Web Growth Facility

During the previous reporting period a new web growth facility, the N-furnace (shown in Figure 18), was constructed.(8) This facility includes all the features required for sustained steady-state web growth. It permits operation under conditions of constant melt level, constant temperature, constant crystal width, thickness, and speed of growth and has provisions for programmed start of web growth.

During the early part of this reporting period, growth runs in the N-furnace were dedicated to achieving the proper furnace adjustments for continuous feeding of a standard width-limiting J98M3A lid and shield assembly combined with the elongated crucible. This configuration, which had been well characterized in the WA and WB furnace facilities, although not with controlled melt level, was adapted for melt replenishment by the addition of feed and laser holes.

When initial testing began, installation of the melt level-sensing circuitry had not yet been completed, so that replenishment was carried out with manually set feed rates. The first step was to establish the end shield settings for various replenishment rates so that sufficiently high temperatures were maintained in the feed compartment of the crucible to melt the pellets at the required rate. At the same time, growth behavior was tested at these shield settings in order to establish what feed rates could be achieved without compromising web growth, i.e., the amount of shielding that could be used without seriously perturbing the temperature distribution in the growth region of the melt. These experiments indicated that for web widths of about 2.5 cm, full replenishment rates could be accomplished without difficulty, but that the shielding required for feed rates needed for 3 cm or greater width could begin to affect the temperature

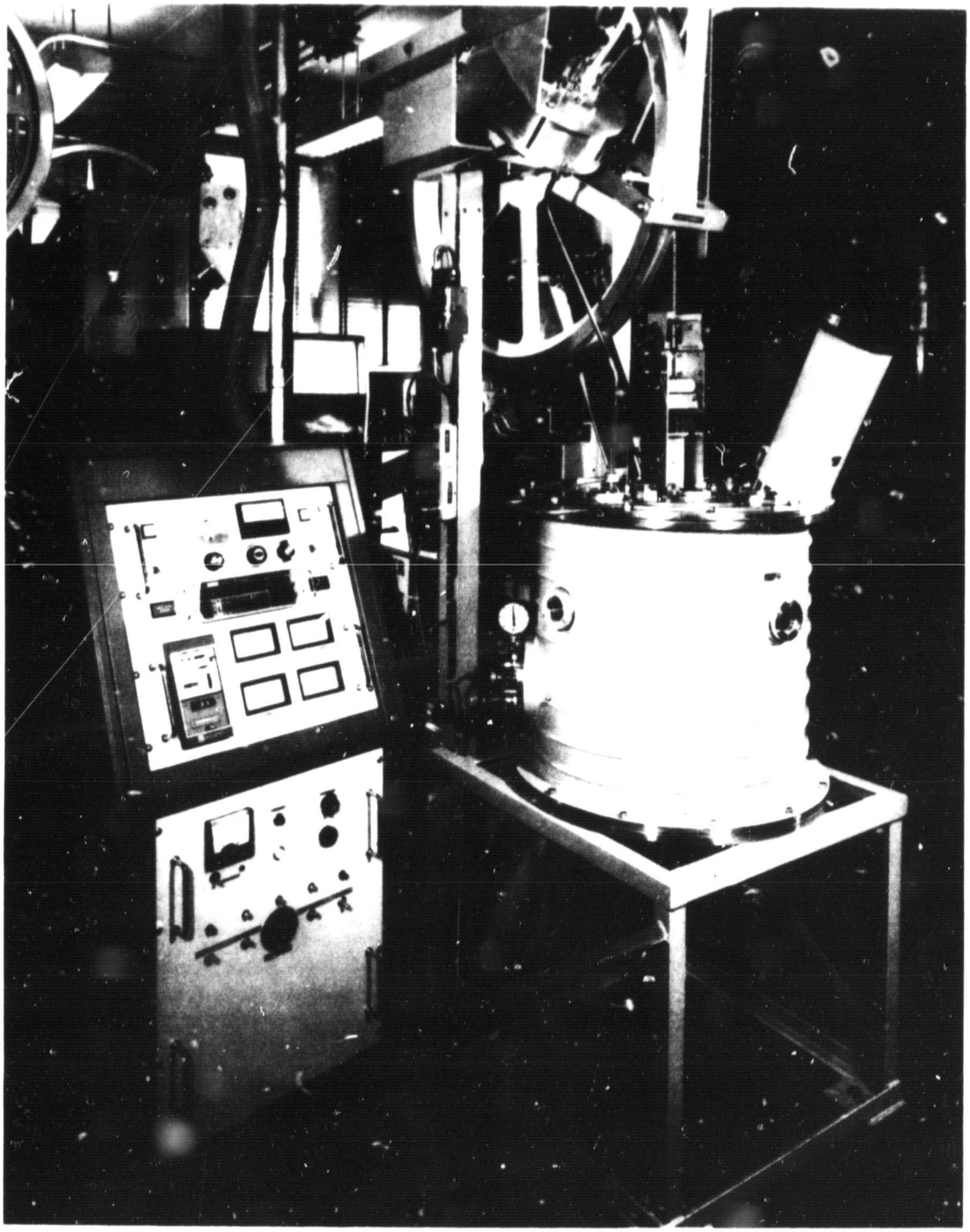

Figure 18. New experimental web growth furnace.

distribution in the growth region adversely. This problem was corrected by a minor modification in the lid geometry.

During this period, installation of the melt level-sensing circuitry was completed and tested during growth experiments. Although the melt level control system components all functioned, it became apparent that the system as a whole was not properly tuned to the growth requirements. Several changes were made in the control loop which brought the response time and loop gain into better agreement with the control requirements, and excellent results were then obtained with actual web growth. In one run, several crystals were grown under automatic level control. During the whole course of the run, all the crystals maintained a constant thickness within about 4 μm (at one constant growth speed) and even the hold temperature did not change by more than a few microvolts. The extreme stability of the growth conditions would indicate that the level control system was operating even better than required.

The modifications made to the N-furnace melt level control system to better meet growth requirements were three in number. First, the time constant of the control loop was made adjustable so that integration periods of 1, 20, 100, and 400 seconds could be used. The faster response times are used for the initial set up of the equipment, but the longer times are needed to avoid unnecessary fluctuations in the final feed rates. With the longer integration times, a higher loop gain can also be used and the response gain of the sensing circuit was increased by a factor of about ten. As a result, the control capabilities of the system are easily of the order of 100 μm or better in melt height sensing. Finally, a selectable limiting speed was placed on the pellet feed motor in order to prevent overfeeding during transient conditions.

At this point, the N-furnace became a web growth research tool capable of generating growth conditions controlled to a degree not previously available.

3.3 Experimental Web Growth

3.3.1 Introduction

The process of developing a functional new growth configuration follows a three-stage progression. The first stage is the thermal modeling, the results of which generate a design for a growth configuration. Stress and buckling models are applied as appropriate when the $(\alpha T)''$ results warrant the effort. The design is then fabricated into hardware and tested experimentally. The objective of this second phase of the progression is to experimentally verify the stress behavior predicted by the model, i.e., to find how wide the crystal can grow before deformation occurs. At this stage, long slots which provide melt temperature profiles compatible with crystal widths of about 6.5 cm are used. Lid and shield temperature measurements are made to verify consistency with the model, and modifications are made as required to produce the desired temperature distribution in the vertical direction. This stage involves a cross interaction between modeling and experiment. The third stage of development is the adaptation of the low-stress configuration for semi-automated growth. This phase is largely empirical, guided by experience. It involves the incorporation of melt replenishment and width control provisions into the design, and the determination of optimum shielding and coil position for good growth at constant width and melt level, i.e., steady-state growth. Only the designs which continue to show promise through the first and second phases reach the third phase.

3.3.2 The J419 and J435 Configurations

The first lid and top shield configuration in which hardware design was generated by the thermal stress modeling results was the J419, discussed in Section 3.1 of this report. The stress characteristics of crystals grown from this configuration agreed extremely well with the predictions of the models, with buckling stresses much lower than those obtained with previous configurations.

Encouraged by the success of the baseline J419 design, a series of variations of this configuration were tested in order to test the sensitivity of growth behavior to variations such as top shield spacing and minor variations in slot geometry and coil position, etc. Lid and shield temperature measurements were made to complement the modeling work. Growth parameters evaluated were growth velocity and residual stress, in addition to the width at which buckling was initiated.

In one series of experiments, the J419 was modified to a more open geometry by beveling the top lid and using a different shield stack order. Although the growth speed was enhanced, there was also a change in the character of the residual stress. Whereas the standard J419 configuration produced crystals with negative residual stress, the modified version gave material with positive residual stress. In both cases, the magnitude could be either very small or moderate, depending on other growth parameters. The higher speed modifications also would grow moderately wide material, up to 40 mm, but tended to deform at slightly narrower widths than the unmodified J419.

The earlier modeling results suggested that the residual stress in some of the higher speed versions of the configuration could be reduced by reducing the heat loss from the web in the interface region. One feature of a lid design which would accomplish this would be a bevel on the bottom edge of the slot in the lid. Thermally, this would allow the web to "see" the hot crucible cavity for a greater portion of its length so that the heat loss near the growth front would be decreased.

Four runs (J439-J442) were made in which the top lid was either unbeveled or had a 3 mm bevel; the bottom lid had either a 1.5 mm or a 3 mm bevel. It was found that the bevel on the bottom of the lid had more effect on speed than on residual stress, while the bevel on the top lid affected the stress more than the speed.

In general, the only modification of the basic design which had a positive effect on growth was a small bevel on the lid slot. Other variations either had little observable effect on growth behavior or generated a negative result. For example, opening the slots in the top shields increased the growth velocity but caused the crystal to degenerate at narrower widths. The model indicated that increasing the height of the top shield stack should further reduce buckling stresses, but this did not seem to have a significant effect with the J419 lid configuration.

While modifications to the J419 configuration were being tested in the J-furnace, experiments in the WA-furnace were directed to testing the compatibility of the J419 configuration with the elongated crucible which would be required for growth at constant melt level. Adjustable end shields were installed. Melt probe data showed that the lateral coil position and the end shield height affect the melt profile differently and that adjustment of both parameters is necessary to obtain a flat, symmetric temperature distribution in the melt. However, when the proper melt temperature profile was achieved, it was established that the low-stress characteristics of the J419 configuration were maintained with the elongated crucible configuration.

At this point it seemed appropriate to combine the wide-growth, low-stress capabilities of the J419 configuration with the width-limiting behavior of the J98M3A configuration for demonstrating extended growth runs. Lids and shields were fabricated which combined these features in a hybrid configuration now known as the J435. Four runs were made with this configuration in the J-Furnace to evaluate the width-limiting capabilities of the design, and the results confirmed a steady growth width between 28 mm and 33 mm, depending on the furnace parameters.

Feed holes and laser holes were then added to the J435 lids and shields and the hardware installed in the N-Furnace with an elongated crucible for melt replenishment. Preliminary experiments focused on optimizing the end shield adjustment and the work coil position so that the melt profile is compatible with both steady-state width and melt replenishment.

Several growth runs were made both with and without melt replenishment. In one run, a 4.8 meter crystal was grown with the width held at 3.1 to 3.3 cm for 3.4 meters. This crystal was grown without replenishment due to clogging of the feed hole with oxide, a problem later resolved. Several 3 to 4 meter long crystals were grown with replenishment, with thickness constant to within a few microns and width limited in the 3.1 to 3.3 cm range.

The J435 configuration was installed in furnaces at the Westinghouse Advanced Energy Systems Division (AESD), replacing the J98M3A configuration, where it could be tested in long (100 hr) growth runs. Long undeformed crystals were produced regularly at widths of 3.3 cm. Additionaly, these crystals had much lower residual stress than crystals grown from the J98M3A configuration, resulting in a significant reduction in breakage during cell processing. While the experiments with the J419 and variations were being carried out, the new temperature model was developed. This model can accommodate complex lid slot designs and any discrete number or spacing of top shields, enormously expanding the range of designs which can be accurately evaluated.

On the basis of results using the new model, combined with experimental correlations and experience with the J419, it was concluded that a new lid slot geometry combined with an extended shield stack should produce significantly lower buckling stresses than the J419 configuration. This new design has been designated the J460 configuration.

3.3.3 The J460 Configuration

The J460 configuration has a combination lid composed of a 9.5 mm thick J352 lid with a recessed slot for the bottom element (L1) and the 6.3 mm thick top section (L2) from the J419 configuration. The intent of the recessed section of the lid was to reduce gas conduction effects and so to emphasize the radiative transfer assumed in the modeling.

During the initial experimental evaluation of this design, web crystals up to 48 mm in width were grown without obvious evidence of buckling. Furthermore, ribbon split measurements indicated very low residual stress levels, even on 41 mm wide samples. The latter data were very encouraging since the residual stress might be expected to increase as the third or fourth power of the ribbon width and thus be fairly high in so wide a crystal.

On the basis of this initial success, the J460 configuration was installed in a furnace at the Westinghouse Advanced Energy Systems Division (AESD) in order to accelerate the accumulation of growth experience. A number of undeformed crystals 5.0 to 5.4 cm in width were grown. These crystals were generally terminated not because of degradation in quality, but because of melt depletion (continuous replenishment was not in use at AESD at that time). Furthermore, the high quality of material grown from the J460 is evidenced by the fact that solar cells fabricated from it have consistently shown efficiencies in the 15 to 16% range.

Having evaluated the basic growth behavior of the J460 configuration, it was then adapted for melt replenishment in order to test growth at known melt levels. The top shields were also instrumented to measure actual shield temperatures at different coil heights for incorporation into the models. A device was constructed to accurately measure melt position so that growth parameters such as the velocity-thickness relationship could be determined at known growth conditions. This work is still continuing.

The next step was to design a width-limiting version of the J460. This design has been completed and will be tested experimentally during the next reporting period.

3.3.4 Long Growth Runs and Oxide Control

As part of a parallel web growth development program funded by Westinghouse AESD, four runs were made in which two furnaces, one of them the N-furnace, were operated 24 hours per day for up to 103 hour long periods to evaluate possible practical problems with continuous melt replenishment for extended times. No fundamental difficulties were encountered with the operation of the equipment. However, some problems with oxide accumulation in the melt sensor laser holes and the feed holes in the top shields were identified. In the case of the feed holes, the dropping pellets served to keep the feed hole clear, but if replenishment was interrupted, oxide tended to accumulate until the hole was blocked.

The oxide accumulation in the laser holes was eliminated by fairly straightforward changes in the geometry of the holes in the shield stack. The solution to the problem of oxide accumulation in the feed holes was more complex and required major changes in the polysilicon feed route through the growth system lids and shield stack. The new design is fully compatible with feed stock pellets prepared in the JPL shot tower developed by Kayex.

These improvements permit melt replenishment to be interrupted at will and growth runs to be carried over to the next day, or several days, without oxide buildup. This in turn increases the amount of growth data which can be obtained in a single run and produces a saving in crucible and silicon costs.

4. SUMMARY, CONCLUSIONS, AND FUTURE WORK

4.1 Summary and Conclusions

The thermal stress models have been successfully applied to the design of new low-stress growth configurations. The J419 and J460 configurations represent the first two steps in achieving substantial reductions in buckling stresses, a factor of three overall, and have yielded substantial increases in the width of high-quality web crystals which have been grown. Growth experiments can now be carried out under controlled and constant growth conditions with the ability to maintain the melt at the desired level through continuous replenishment. The combination of thermal modeling with carefully controlled experiments can be expected to produce further substantial increases in the area throughput of web crystal of the quality required for high-efficiency solar cells.

4.2 Future Work

Thermal modeling combined with experimental evaluation will continue to be applied to the design of lower stress, higher throughput growth configurations. In addition, we will be studying dynamic thermal trimming as a method for optimizing both the requirements for growth during the initial transient involving the start of growth and widening to desired width, and for growth at steady-state for increased area throughput. Initial efforts will be directed toward changes in melt level and the position of the top shields during web growth. Both parameters affect both stress and growth velocity, as well as the quality of crystal start. Thus, the objective would be to change the configuration during growth to match the thermal requirements at each stage. Additional configurational parameters will be examined as results and experience dictate.

5. NEW TECHNOLOGY

No new technology is reportable during this period.

6. REFERENCES

1. C. S. Duncan, et al. Silicon Web Process Developments. Annual Report. April 1978-April 1979. DOE/JPL 954654-79/2 p. 90.

2. R. G. Seidensticker and R. H. Hopkins, J. Crystal Growth, 50, 221 (1980).

3. C. S. Duncan et al. Silicon Web Process Development. Annual Report. April 20, 1977-April 19, 1978. DOE/JPL 954654-78/1. p. 195.

4. C. S. Duncan et al. Silicon Web Process Development, Annual Report. (June 30, 1980). DOE/JPL-954654-80/11. p. 44.

5. C. D. Graham, et al. Final Report-Research and Development of Low Cost Processes for Integrated Solar Arrays. No. ERDA/SE/EC(11-1)-2721/FR/76/1.

6. B. A. Boley and J. H. Weiner: Theory of Thermal Stresses (New York: Wiley, 1960) p. 323.

7. C. S. Duncan et al. Large Area Sheet Task. Advanced Dendritic Web Growth Development. Annual Report: October 23, 1980 to October 22, 1981. DOE/JPL-955843/82/1. p. 43.

8. Ibid., pp. 63ff.

7. ACKNOWLEDGEMENTS

We would like to thank H. C. Foust, E. P. A. Metz, L. G. Stampahar, S. Edlis, W. B. Stickel, and W. Chalmers for their contributions to the web growth studies. We would also like to thank the staff of the Analytical Mechanics Department, especially David Augustine, for assistance in the application of the WECAN code to our analysis. Additionally, we thank Renee B. Feldman for modifying and improving the graphics routines in the models. We further acknowledge the expertise of Georgia Law in the editing and Debbie Todd the typing of the manuscript.

APPENDIX I

Web Temperature Computer Model

1. INTRODUCTION

Thermal stress and buckling modeling of dendritic web crystals requires temperature distribution data along the growing web. Because of the difficulty of measuring web temperature, we instead compute it from the furnace lid and shield geometry and temperature distribution. This computation is performed by a computer code called "RIBBON" which integrates the required heat transfer equation for the given radiative web environment. A description of this program and data input follows.

2. CONSTRUCTION OF MODEL

2.1 Differential Equation

The purpose of the RIBBON program is to determine the temperature, T, of the growing silicon web as a function of the distance, x, from the lower edge of the furnace lid. RIBBON accomplishes this task by integrating the heat conduction equation:

$$\rho \; CpV \frac{dT}{dx} = \frac{d}{dx} \left(\frac{a}{T} \frac{dT}{dx}\right) - \frac{2q}{b} \qquad \text{[A-1]}$$

where ρ = density

Cp = specific heat

V = web pull velocity

a = 318 W/cm

b = web thickness

q = heat flux from one side of the web.

One of the major tasks of the RIBBON program is to calculate the geometric form factors for the term "q". A detailed discussion of this computation is found in the last quarterly report (DOE/JPL-955843/82/6). For the purpose of recognizing the degree of nonlinearity of equation A-1, we note that q can be expressed in the form

$$q = \sigma E T^4 + f(x),$$

where σ is the Stephan-Boltzman, E is the emissivity of silicon web, and f(x) is a function of position x on the web and the geometry and temperatures of the lid and shields of the furnace. Above 20 cm from the lid, the web enters a chimney and thus no longer "sees" the lid and shields. For a simple approximation, we say that it "sees" only the ambient temperature, T_a. Thus, for $x > 20$ cm,

$$q = \sigma \varepsilon \left(T^4 - T_a^4\right) \qquad [A-2]$$

The longer the ribbon grows, the closer its temperature approaches the ambient. This fact together with the initial condition that the web starts to grow at the silicon melt temperature, $T_m = 1685^oK$, gives us the boundary conditions

$$\begin{aligned} T(x_o) &= T_m \\ T(\infty) &= T_a \ . \end{aligned} \qquad [A-3]$$

The position $x = x_o$ is the growth front and has a value equal to the negative of the input parameter LIN in the program.

Differential equations with boundary conditions are more difficult to solve than those with initial conditions; they generally must be solved iteratively. Since most numerical integration routines are written for first order equations, we transform the second order equation (A-1) into two first order equations with the substitutions:

$$u_2 = \rho \ Cp \ V \ T_m/a$$
$$\beta_2 = \varepsilon\sigma \ T_m{}^4/(ab)$$
$$TT(1) = T/T_m$$
$$TT(2) = \frac{dT}{dx} (1/T) \qquad [A-4]$$

Equation A-1 can be expressed now as a system of first order equations:

$$TTP(1) = TT(1) \cdot TT(2)$$
$$TTP(2) = u_2 \ TTP(1) + \beta_2 Q$$

where

$$TTP(i) = \frac{d}{dx} [TT(i)] \qquad i = 1,2$$

and

$$Q = 2q/\varepsilon\sigma \quad . \qquad [A-5]$$

The nonlinearity of these equations makes them unstable as small errors in the steps of the integration are quickly magnified in the succeeding steps. We tried several different methods of numerical integration but found the simple fourth order Runge-Kutta method to be the most stable. Even so it is necessary to use double precision to obtain reasonable results. In practice, an initial slope of the temperature is guessed. If the slope leads to a curve which gives below the ambient temperature, then the slope is increased for the next guess. If the resulting curve goes above the silicon melt temperature, then the initial slope is decreased. This iteration continues until the double precision accuracy of the choice of initial slope is exhausted; in other words, there is no way to choose an initial slope between the high slope and the low slope since they are identical to 16 places. Generally, the integration curve does not blow up (or down) until 20 - 30 cm. In this case the integration from 0 to 10 cm (the length of the buckling finite element model) is fairly accurate. If it blows up before this length, this may no longer be true. (A smaller integration step size, HO, may improve this problem.) Also, if the integration remains between the melt and ambient temperature for a longer length, the integration may not be accurate because other values of the initial slope may lead to different temperature curves which also remain bounded. The boundary condition, $T(\infty) = T_a$, must then be applied. Thus, it becomes necessary to examine the asymptotic expansion of equations A-1 and A-2. While the numerical integration of equation A-1 or equation A-4 starting with initial values at the melt interface will be accurate for small values of x, the asymptotic expansion can be expected to be accurate for large values of x. Hopefully, their regions of accuracy will overlap; if this is not the case for some problems, then some approximation to an intermediate solution might be required.

2.2 Asymptotic Expansion

For large x, it is most convenient to change the differential equations A-1 and A-2 into a system of first order equations with the following substitutions:

$$\begin{aligned} \alpha &= \rho \, CpV \, T_a/a \\ \gamma &= 2\varepsilon\sigma \, T_a^{\,4}/ab\alpha^2 \\ y_1 &= T/T_a \\ y_2 &= (1/\alpha T) \frac{dT}{dx} \end{aligned} \qquad [A-6]$$

Thus,

$$\begin{aligned} \frac{dy_1}{dx} &= \alpha \, y_1 \, y_2 \\ \frac{dy_2}{dx} &= \alpha \, y_1 \, y_2 + \gamma\alpha \, (y_1^{\,4} - 1) \end{aligned} \qquad [A-7]$$

If one attempts a formal power series solution of equation A-7 in negative powers of x (so that they are finite as x approaches infinity), one would obtain the trivial solution $Y_1 = 1$ and $Y_2 = 0$. This solution, however, does not give the general asymptotic expansion of equation A-7. Theory (Wolfgang Wason, Asymptotic Expansions for Ordinary Differential Equations, Interscience, N.Y., 1965) shows that the general solution is a function of two parameters: $C \exp \alpha x(1-\sqrt{1+16\gamma})/2$ and $D \exp \alpha x(1+\sqrt{1+16\gamma})/2$, where C and D are arbitrary constants. Since the second parameter becomes infinite as x approaches infinity, we let D vanish and look for functions of the first parameter. The substitution

$$\xi = \exp\ [\alpha x(1-\sqrt{1+16\gamma})/2]$$

transforms the equation A-6 into

$$\begin{aligned} y_1' \,\xi\, (1 - \sqrt{1+16\gamma}) &= 2\, y_1 y_2 \\ y_2' \xi\, (1 - \sqrt{1+16\gamma}) &= 2\, y_1\, y_2 + 2\gamma\, (y_1^4 - 1) \end{aligned} \qquad [A-8]$$

where the primes represent differentiation with respect to the variable ξ. We can now seek a power series solution of equation A-8 in the form

$$\begin{aligned} y_1 &= a_{10} + a_{11}\,(C\xi) + a_{12}\,(C\xi)^2 + \ldots \\ y_2 &= \phantom{a_{10} +{}} a_{21}\,(C\xi) + a_{22}\,(C\xi)^2 + \ldots \end{aligned} \qquad [A-9]$$

where $a_{10} = 1$ from the boundary condition and a_{11} may also be chosen equal to unity since C is an arbitrary constant. Equating the coefficients of $(C\xi)^n$ on both sides of equation A-8, we obtain

$$\begin{aligned} n\, a_{1n}\, (1 - \sqrt{1+16\gamma}) &= 2 \sum_{m=0}^{n-1} a_{1m}\, a_{2(n-m)} \\ n\, a_{2n}\, (1 - \sqrt{1+16\gamma}) &= 2 \sum_{m=0}^{n-1} a_{1m}\, a_{2(n-m)} + 2\gamma\, [b_{n/2}^{\,2} + 2 \sum_{m=0}^{(n/2)\,-1} b_m\, b_{n-m}] \end{aligned} \qquad [A-10]$$

for n even or

$$na_{2n}\ (1-\sqrt{1+16\gamma}) = 2\sum_{m=0}^{n-1} a_{1m}\ a_{2(n-m)} + 4\gamma \sum_{m=0}^{(n-1)/2} b_m\ b_{n-m} \qquad [A-10]$$

for n odd,

where

$$b_i = a_{1(i/2)}{}^2 + 2\sum_{j=0} a_{ij}\ a_{1(i-j)} \quad ,\ i\ \text{even}$$

$$= \sum_{j=0}^{(i-1)/2} a_{1j}\ a_{1(i-j)} \quad ,\ i\ \text{odd}$$

$$b_o = 1$$

From these equations, the a_{1n} and a_{2n} are determined from the values of a_{1m} and a_{2m}, where $m < n$. In this way, we find the coefficients of the asymptotic expansion A-9. The radii of convergence of these power series may be found from the formulas:

$$R = \text{Lim}\ |\ a_n/a_{n+1}\ |\ \text{if it exists}$$

$$\text{and}\quad \underset{n\to\infty}{\text{Lim sup}}\ |\ a_n\ |^{1/n} = \alpha = 1/R$$

The next steps in the procedure are to choose a value of C and then a value of $\xi > 20$ cm. such that equation A-9 converges. From equations A-4, A-6, and A-9, initial conditions for equation A-5 may be found at the value of x corresponding to that of ξ. Equation A-5 can now be integrated backward to $x = x_o$ using the same Runge-Kutta method as before. These steps are interated by increasing or decreasing the choice of C accordingly as $T(x_o)$ is less than or greater than T_m.

3. COMPUTER PROGRAM INPUT/OUTPUT OPTIONS

The input parameters of the RIBBON program are divided into two sets -- the first to define the geometry and the second everything else. In this way, Calcomp plots may be obtained for any number of geometric configurations in each run. In each plot, up to three different graphs (black, green, and red) of the second derivative of αT can be obtained for different nongeometric parameters of web growth run.* A sample Calcomp plot is illustrated in Figure 2. Besides the αT second derivative curves, it diagrams the lid and shield geometry.

The following input records are read in the first data set. The data are read in free field format with either spaces or commas separating them. Variables beginning with I-N are integers (except for LIN) and all others are double precision.

RECORD 1:

IGRAPH = Input 0 if there are to be no Calcomp graphs in the run, otherwise input 1.

RECORD 2:

NS = Number of geometric elements. These include the lid, the shields, and their separating gaps.

JQC = Parameter to correspond to the type of WECAN element

= 2 for quadratic elements

= 3 for cubic elements

JN = Number of WECAN elements in the x direction (generally has been set to 23).

NE = Number of WECAN elements in the y direction (generally has been 5 for two-dimensional elements and 7 for three-dimensional ones).

---

*Here α stands for the thermal expansion of silicon and is represented by ALPO + ALPI * TEMP in the program; it is unrelated to the α in equations A6 and A7.

NG = One plus the number of data sets for a given geometry.

LIN = Distance (cm) of the growth front below the lower edge of the lid.

EMAG = Magnification of the JNth element in the x direction relative to the first WECAN element at the growth front (generally has been 8).

ELL = Length of ribbon modeled on WECAN in centimeters (generally has been 10).

RECORD 3:

H(I),I = 1, NS = Height (cm) of ith horizontal surface above the lower surface of the lid.

RECORD 4:

Y(I), I = 0, ..., NS+1 = Half width (cm) of the central gap of the ith horizontal surface.

The H and Y parameters are illustrated in Figure 3. This completes the first data set.

The second data set consists of the following records:

RECORD 1:

IS = 1 for forward integration

= -1 for backward integration from asymptotic expansion (not yet implemented).

HO = integration step size (generally set to 0.01).

KOUT = 6 for printed temperature data in WECAN stress input formalism

= 7 for punched WECAN data.

KOU = 0 for no plot of the αT second derivative.

= 1 for a plot

EPS = emissivity of silicon web.

A = thermal conductivity of silicon multiplied by its temperature (318 W/cm).

B = web thickness (cm).

V = web pull velocity (cm/min)

POMIN = minimum initial value of TT(2). If not known, set to -1.

POMAX = maximum initial value of TT(2). If not known, set to -0.01.

CMIN = minimum value of the parameter in equation (A-9). If not known, try 1.

CMAX = maximum value of the parameter C. If not known, try 20.

RECORD 2:

TS(I),I = 1, ... , NS+1 = Temperature (degrees Kelvin) of the ith geometric element.

These RECORDS 1 and 2 may be repeated up to a total of three sets. The data sets 1 and 2 can be repeated an indefinite number of times.

APPENDIX II
Computer Code Listing

```
@RUN, /RNPT JSS05,09F40READY20,SCHRUBEN,5,100/1500

@HDG  RIBBON

@FTN,SDFIV
FTN 8R1W4 08/25/82-20:50
   C     SILICON WEB - ANALYSIS OF HEAT LOSS OF MOVING WEB
         IMPLICIT DOUBLE PRECISION (A-H,O-Z)
         DOUBLE PRECISION LIN,LAMB,TS(0:20),H(0:20),Y(0:20),XS(0:100),
        1     X(0:60)
         DIMENSION TT(2),TS4(20),T(100),TP(100),TPP(100),ATPP(100),Y2(
        1     ,TTP(2)
         INTEGER  IXS(40),ISR(0:60,20)
         INTEGER  TITLE(11),LABELX(2),LABELY(2),ICOLOR(4)
         REAL XR(150),YR(4,150),XLEN
   C     THE ABOVE ARE GRAPH PARAMETERS
         COMMON /CNI/ U2,BETA2,ISR,TS4,Y2,H,ICHIM,NS,NS1
         COMMON /CNJ/ TA,IFLAG
         DATA TITLE/'SECO','ND D','ERIV','ATIV','E OF',' ALP','HA*T',
        1     'EMPE','RATU','RE*5','00'/
         DATA LABELX/'X-AX','IS'/
         DATA LABELY/'Y-AX','IS'/
         DATA ICOLOR/1,1,2,3/
         KI= 5
         KO= 6
   C     IGRAPH = 0  FOR NO CALCOMP
   C            = 1  FOR SOME CALCOMP
   C     NG IS ONE PLUS NUMBER OF DATA SETS FOR A GIVEN GEOMETRY (4 MA
   C     NS IS NUMBER OF SHIELDS PLUS LID SECTIONS PLUS GAPS INBETWEEN
   C     TS(I) IS THE TEMPERATURE OF THE ITH SHIELD OR GAP
   C     H(I) IS THE HEIGHT OF THE ITH HORIZONTAL SURFACE ABOVE THE LO
   C     SURFACE OF THE LID
   C     Y(I) IS THE DISTANCE OF SHIELD EDGE TO WEB
   C     (Y(0) IS HALF-WIDTH OF MELT SURFACE, Y(1) IS HALF GAP OF LID,
   C      Y(NS) IS DISTANCE OF INNER EDGE OF TOP SHIELD TO WEB,
   C      Y(NS+1) IS DISTANCE OF OUTER EDGE OF TOP SHIELD TO WEB)
   C     JQC=2 FOR QUADRATIC ELEMENTS
   C        =3 FOR CUBIC ELEMENTS
   C     IS=1 FOR FORWARD INTEGRATION
   C       =-1 FOR BACKWARD INTEGRATION
   C     JN IS NUMBER OF ELEMENTS IN A ROW ALONG THE WEB AXIS
   C     LIN IS DISTANCE OF GROWTH FRONT BELOW LID
   C   -LIN .GT. X(0)
   C     EMAG IS MAGNIFICATION OF LAST ELEMENT RELATIVE TO FIRST NEXT
   C     ELL IS LENGTH OF WEB TO BE MODELED
   C WE ASSUME  ELL < 20
   C     NE= 5  FOR 2D ELEMENTS
   C     NE= 7  FOR 3D ELEMENTS
         TS(0)= 1685.D0
         TM= 1685.D0
         TMR= 1./TM
         LAMB= 1804.D0
         TM4= TM**4
         CP= 0.9811D0
         RHO= 2.30D0
         SIGMA= 5.67D-12
         H(0)= 0
         X(0)= -1
         ISR(0,0)= 0
         X0= X(0)
         ISR(0,1)= 1
         XS(0)= X0
         READ(KI,*) IGRAPH
         IF (IGRAPH .GT. 0) CALL PLOTIN(1.,1.)
         YR(1,1)= -1
         XR(1)= -1
         XR(2)= -1
         DO 998 ISUPER=1,10
1        READ(KI,*,END=999) NS,JQC,JN,NE,NG,LIN,EMAG,ELL
1        WRITE(KO,5) NS,JQC,JN,NE,NG,LIN,EMAG,ELL
1      5 FORMAT('0 NS=',I4,' JQC=',I4,' JN=',I4,' NE=',I4,' NG=',I4,
1       1     ' LIN=',E12.5,' EMAG=',E12.5,' ELL=',E12.5)
1        NS1= NS+1
1        H(NS1)= 20
```

```
1             READ(KI,*) (H(I),I=1,NS)
1             WRITE(KO,7) (H(I),I=1,NS)
1           7 FORMAT('0H=',/,(E14.5))
1             READ(KI,*) (Y(I),I=0,NS1)
1             WRITE(KO,8) (Y(I),I=0,NS1)
1           8 FORMAT('0Y=',/,(D14.5))
1             DO 10 I= 0,NS1
2             Y2(I)= Y(I)**2
2          10 CONTINUE
1             YR(1,2)= SNGL(Y(0))
1             ALP0= 2.8457E-6
1             ALP1= 9.796E-10
1             ALP2= 2*ALP1
1             K= 0
1             DO 50 I= 2,NS
2             I1= I-1
2             XLS= X0
2     C       XLS IS THE LOWER BOUND OF TS(I) RADIATION ON WEB
2             HI= H(I)
2             YI= Y(I)
2             DO 20 J= 1,I1
3             IF (YI .GT. Y(J)) THEN
4                   TEMP= (H(J)*YI-Y(J)*HI)/(YI-Y(J))
4                   IF (TEMP .GT. XLS) XLS= TEMP
4             END IF
3          20 CONTINUE
2             IF (XLS .LE. X0) THEN
3                   ISR(0,I)= 1
3             ELSE
3                   ISR(0,I)= -1
3                   DO 25 J=K,0,-1
4                   J1= J+1
4                   IF (XLS .GE. XS(J)) THEN
5                         XS(J1)= XLS
5                         IXS(J1)= I
5                         GO TO 26
5                   ELSE
5                         XS(J1)= XS(J)
5                         IXS(J1)= IXS(J)
5                   END IF
4          25       CONTINUE
3          26       K= K+1
3             END IF
2             XUS= 20
2     C       XUS IS THE UPPER BOUND OF TS(I1) RADIATION ON WEB
2             HI= H(I-2)
2             YI= Y(I1)
2             DO 30 J= I,NS
3             J1= J-1
3             IF (YI .GT. Y(J))  THEN
4                   TEMP= (YI*H(J1)-HI*Y(J))/(YI-Y(J))
4                   IF (TEMP .LT. XUS) XUS= TEMP
4             END IF
3          30 CONTINUE
2             IF (XUS .LT. 20) THEN
3                   DO 35 J= K,0,-1
4                   J1= J+1
4                   IF (XUS .GE. XS(J)) THEN
5                         XS(J1)= XUS
5                         IXS(J1)= I1
5                         GO TO 36
5                   ELSE
5                         XS(J1)= XS(J)
5                         IXS(J1)= IXS(J)
5                   END IF
4          35       CONTINUE
3          36       K= K+1
3             END IF
2          50 CONTINUE
1             IB= 0
1             I= 0
1             DO 70 L= 1,K
2          60 IF (XS(L)-X(I) .LT. 1.D-4) THEN
3             IXSL= IXS(L)
3                   ISR(I,IXSL)= -ISR(I,IXSL)
3                   GO TO 70
```

```
3              END IF
2              I1= I
2              I= I+1
2              DO 65 J= 0,NS
3          65  ISR(I,J)= ISR(I1,J)
2              IF (H(IB)-XS(L) .GT. 1.D-4) THEN
3                      X(I)= XS(L)
3              IXSL= IXS(L)
3                      ISR(I,IXSL)= -ISR(I,IXSL)
3              ELSE
3                      X(I)= H(IB)
3                      IB= IB+1
3                      ISR(I,0)= IB
3                      GO TO 60
3              END IF
2          70  CONTINUE
1              DO 80 L= IB,NS
2              IF (H(L) .LT. X(I)) GO TO 81
2              I1= I
2              I= I+1
2              X(I)= H(L)
2              DO 75 J= 1,NS
3          75  ISR(I,J)= ISR(I1,J)
2          80  ISR(I,0)= L+1
1          81  CONTINUE
1              LAS= I
1              IF (X(I) .NE. 20) THEN
2              LAS= I+1
2              X(LAS)= 20
2              END IF
1              LAS= LAS+1
1              X(LAS)= 30
1              WRITE(KO,1000)(X(J),J=0,LAS)
1              WRITE(KO,1001)(XS(J),IXS(J),J=1,K)
1              WRITE(KO,1002)((ISR(L,J),J=0,NS),L=0,I)
1              DO 90 I= 1,LAS
2              K= I
2              IF((X(I)+LIN).GT. 1.D-8) GO TO 91
2          90  CONTINUE
1          91  CONTINUE
1              KO= K
1              RA= EMAG**(1.D0 /(JN-1))
1              EL= ELL*(1-RA)/(1-RA**JN)
1              JNN= JQC*JN+1
1              KK= 2
1              DO 110  KKI= 0,K
2              KKKS= KKI+1
2              KKK= KKI
2              IF((H(KKI)+LIN) .GE.  0.  ) GO TO 111
2              KK= KK+1
2              XR(KK)= SNGL(H(KKI))
2              YR(1,KK)= SNGL(Y(KKI))
2              KK= KK+1
2              XR(KK)= SNGL(H(KKI))
2              YR(1,KK)= SNGL(Y(KKKS))
2         110  CONTINUE
1         111  KKS= KK
1              KKS1= KK+1
1              DO 997  IC= 2,NG
2              READ(KI,*) IS,HO,KOUT,KOU,EPS,A,B,V,POMIN,POMAX,CMIN,CM
2              WRITE(KO,82) IS,HO,KOUT,KOU,EPS,A,B,V,POMIN,POMAX,CMIN,
2        C     KOUT = 6 FOR PRINTED STRESS DATA
2        C          = 7 FOR PUNCHED STRESS DATA
2        C     KOU > 0 FOR GRAPH
2          82  FORMAT('0 IS=',I3,' HO=',E12.5,
2           1              ' KOUT=',I3,' KOU=',I3,' EPS= ',E12.5,' A= ',E1
2            2           E12.5,' V= ',E12.5,/,' POMIN= ',D25.18,' POMAX=
2            3           /,' CMIN= ',D25.18,' CMAX= ',D25.18)
2              READ(KI,*) (TS(I),I=1,NS1)
2              WRITE(KO,6) (TS(I),I=1,NS1)
2           6  FORMAT('0TS=',/,(D14.4))
2              DO 83  I= 0,NS1
3              TS(I)= TS(I)*TMR
3              TS4(I)= TS(I)**4
3          83  CONTINUE
2              IS1= MOD(1-IS,JQC)
```

```
2             HO= HO*IS
2             TA= TS(NS1)
2             V= V/60
2             BETA2= EPS*SIGMA*TM4/(A*D)
2             BETA=  DSQRT(2*BETA2)
2             U2= RHO*CP*V*TM/A
2             DO 101 J= 1,500
3             IFLAG= 0
3             K= KO
3             DX= EL/JQC
3             IF (IS .EQ. -1) GO TO 400
3             TT(1)= 1
3             XX= -LIN
3             POOO= .500*(POMAX+POMIN)
3             IF  (POOO .EQ. POO .AND. J .NE. 1)      GO TO 102
3             POO= POOO
3             TT(2)= POO
3             KK= KKS+1
3             KKK= KKKS-1
3             I1= 1
3             I2= JNN-1
3             X2= -LIN
3             ICHIM=    1
3             GO TO 409
3        400  CONTINUE
3        409  CONTINUE
3             TEMP= TT(1)*TM
3             TEMPP= TT(2)*TEMP
3             DO 450 I=I1,I2,IS
4             X1= X2
4             X2= X1+DX
4             IF (I .EQ. 2 .AND. IS .EQ. -1) X2= X(1)
4             KFLAG= 0
4             T(I)= TEMP
4             TP(I)= TEMPP
4             XS(I)= X1
4             IF (IS*(X(K)-X2)) 410,411,412
4        410  CALL FCNJ(X1,X(K),TT,TTP,HO,K)
4             IF (IFLAG .NE. 0) GO TO 600
4             XR(KK)= SNGL(X1)
4             TEMPPP= TEMP*TTP(2)+TEMPP*TEMPP/TEMP
4             ATEM= (ALPO+ALP2*TEMP)*TEMPPP+ALP2*TEMPP*TEMPP
4             TEMP= TT(1)*TM
4             TEMPP= TT(2)*TEMP
4             YR(IC,KK)= AMAX1(-1.,AMIN1(8.,SNGL(ATEM)*500.))
4             IF (KFLAG .EQ. 0) THEN
5             TPP(I)= TEMPPP
5             ATPP(I)= ATEM
5             END IF
4             IF  (H(KKK) .EQ. X1) THEN
5                   KKK= KKK+1
5                   KK= KK+1
5                   XR(KK)= SNGL(X1)
5                   YR(IC,KK)= YR(IC,KK-1)
5             END IF
4             KK= KK+1
4             KFLAG= 1
4             X1= X(K)
4        411  K= K+IS
4             IF  (IS*(X(K)-X2)) 410,411,412
4        412  CALL FCNJ(X1,X2,TT,TTP,HO,K)
4             IF (IFLAG .NE. 0) GO TO 600
4             TEMPPP= TEMP*TTP(2)+TEMPP*TEMPP/TEMP
4             ATEM= (ALPO+ALP2*TEMP)*TEMPPP+ALP2*TEMPP*TEMPP
4             TEMP= TT(1)*TM
4             TEMPP= TT(2)*TEMP
4             XR(KK)= SNGL(X1)
4             YR(IC,KK)= AMAX1(-1.,AMIN1(8.,SNGL(ATEM)*500.))
4             IF  (H(KKK) .EQ. X1) THEN
5                   KKK= KKK+1
5                   KK= KK+1
5                   XR(KK)= SNGL(X1)
5                   YR(IC,KK)= YR(IC,KK-1)
5             END IF
4             KK= KK+1
4             IF  (KFLAG .NE. 0) GO TO 450
```

```
4            TPP(I)= TEMPPP
4            ATPP(I)= ATEM
4        450 IF (MOD(I,JQC) .EQ. IS1) DX= DX*RA**IS
3            CALL FCNI(X2,TT,TTP,K)
3            I3= I2+IS
3            T(I3)= TT(1)*TM
3            I= I3
3            XS(I)= X2
3            TP(I)= TT(2)*T(I)
3            TPP(I)= T(I)*(TT(2)**2+TTP(2))
3            ATPP(I)= (ALP0+ALP2*T(I))*TPP(I)+ALP2*TP(I)**2
3            XR(KK)= SNGL(X2)
3            YR(IC,KK)= AMAX1(-1.,AMIN1(8.,SNGL(ATPP(I))*500.))
3            IF (IS .EQ. -1) GO TO 600
3            DO 500 JK= K,LAS
4            IF (JK .EQ. LAS) ICHIM= 0
4            CALL FCNJ(X2,X(JK),TT,TTP,H0,JK)
4            IF (IFLAG .NE. 0) GO TO 600
4            X2= X(JK)
4        500 CONTINUE
3        600 CONTINUE
3        780 WRITE(KO,1002) IFLAG
3            WRITE(KO,1005) X1,X2,TT,P00,C
3       1005 FORMAT(3D25.18)
3            IF (IS .EQ. -1) GO TO 95
3            IF (IFLAG) 93,92,94
3         92 GO TO 102
3         93 POMIN= P00
3            GO TO 101
3         94 POMAX= P00
3            GO TO 101
3         95 CONTINUE
3        101 CONTINUE
2        102 VV= -60*A*    P00/(RHO*LAMB)
2            WRITE(KO,7100) VV
2       7100 FORMAT('1',5X,'VV= ',E14.7)
2            DO 849 I=1,5
3            YIELD= 2.57E-11*EXP(49459/T(I))
3        849 WRITE(KO,8490) YIELD
2       8490 FORMAT('   YIELD= ',E15.8)
2            DO 852 I=1,JNN
3        852 WRITE(KO,1000)XS(I),T(I),TP(I),TPP(I),ATPP(I)
2            DO 850 I=1,JN
3            II= JQC*(I-1)+1
3            T1= T(II)
3            T2= T(II+1)
3            T3= T(II+2)
3            T4= T(II+3)
3            DO 800 J=1,NE
4            II= J+(I-1)*NE
4            IF (JQC .EQ. 3) GO TO 795
4            WRITE(KOUT,1006) II,T1,T1,T3,T3,T1
4            IF (NE .EQ. 5) THEN
5                  WRITE(KOUT,1008) T2,T3,T2
5            ELSE
5                  WRITE(KOUT,1007) T1,T3,T3,T1,T2,T3,T2,T1,T1,T3
5                  WRITE(KOUT,1008) T3,T1,T2,T3,T2
5            END IF
4            GO TO 800
4        795 WRITE(KOUT,1006) II,T1,T1,T4,T4,T1
4            WRITE(KOUT,1007) T2,T4,T3,T1,T3
4            WRITE(KOUT,1008) T4,T2
4        800 CONTINUE
3        850 CONTINUE
2            YR(IC,1)= 8
2            DO 860 KKI= 2,KKS
3            YR(IC,KKI)= YR(IC,KKS+1)
3        860 CONTINUE
2        997 CONTINUE
1            ISW= -1
1            K= KKKS-1
1            DO 865 KKI= KKS1,KK
2            IF (XR(KKI) .NE. SNGL(H(K))) THEN
3                  YR(1,KKI)= YR(1,KKI-1)
3            ELSE
3                  K= K+ MAXu(0,ISW)
```

```
3                   YR(1,KKI)= SNGL(Y(K))
3                   ISW= -ISW
3              END IF
2          865 CONTINUE
1              DO 866  I= 1,KK
2          866 WRITE(KO,1009)  XR(I),(YR(J,I),J=1,NG)
1              XLEN=  1.-SNGL(LIN) +ELL
1              IF (KOU .GT. 0) CALL GRAPH(XR,YR,NG,4,KK,XLEN,9.,0,0,TITLE,42,
1             1                                  LABELX,6,LABELY,6,0,0,ICOLOR)
1          998 CONTINUE
           999 CONTINUE
               IF (IGRAPH .GT. 0) CALL PLOT(0.,0.,999)
          1000 FORMAT(8D15.8)
          1001 FORMAT(7(D15.8,I3))
          1002 FORMAT(30I4)
          1006 FORMAT(I6,12X,5F12.4,'       +')
          1007 FORMAT(18X,5F12.4,' +')
          1008 FORMAT(18X,5F12.4)
          1009 FORMAT(8E15.8)
               CALL EXIT
               END
```

```
  RIBBON FCNI

RAYS*RIBBON(1).FCNI(0)
                  SUBROUTINE FCNI(X,TT,TTP,K)
                  IMPLICIT DOUBLE PRECISION (A-H,O-Z)
                  DIMENSION  TT(2),TTP(2),TS4(20),Y2(0:20),ISR(0:60,20),H(0:2
                  COMMON /CNI/ U2,BETA2,ISR,TS4,Y2,H,ICHIM,NS,NS1
                  K1= K-1
                  TTP(1)= TT(2)*TT(1)
                  Q= 2*(TT(1)**4-TS4(NS1)     )
                  IF (ICHIM .EQ. 0) GO TO 100
                  Q= Q+TS4(NS1)-1
                  T4= 1
                  N= ISR(K1,0)
                  N1= N+1
                  DO 50  KK =1,N
                  IF (ISR(K1,KK) .LT. 0) GO TO 50
                  XX= H(KK-1)-X
                  Q= Q+ (TS4(KK)-T4)*XX/DSQRT(XX*XX+Y2(KK))
                  T4= TS4(KK)
               50 CONTINUE
                  XX= H(N)-X
                  Y2K= Y2(N)
                  DO 60 KK=  N1,NS
                  IF (ISR(K1,KK) .LT. 0) GO TO 60
                  Q= Q+ (TS4(KK) -T4)*XX/DSQRT(XX*XX+Y2K)
                  XX= H(KK)-X
                  Y2K= Y2(KK)
                  T4= TS4(KK)
               60 CONTINUE
                  Q= Q+ (TS4(NS1)-T4)*XX/DSQRT(XX*XX+Y2K)
              100 TTP(2)= U2*TTP(1)+BETA2*Q
                  RETURN
             1000 FORMAT(8E15.8)
                  END

@RJEFIN:    RJESPF.RJEFIN . . .

@SS-PPF-SS.RJESFIN
```

RIBBON FCNJ

```
RAYS*RIBBON(1).FCNJ(0)
                  SUBROUTINE   FCNJ(Z1,Z2,Y,YP,H0,K)
                  IMPLICIT DOUBLE PRECISION (A-H,O-Z)
                  DIMENSION Y(2),YT(2),PY(2),YP(2)
                  COMMON /CNJ/ TA,IFLAG
                  Z= Z1
                  H= H0
                  NI= DMAX1(1,IDINT((Z2-Z1)/H)        )
                  DO 500 I= 1,NI
                  IF (I .EQ. NI) H= Z2-Z
                  HH= H*.5D0
                  CALL FCNI(Z,Y,PY,K)
                  IF (I .EQ. 1) THEN
                        YP(1)= PY(1)
                        YP(2)= PY(2)
                  END IF
                  RK1 = H*PY(1)
                  RL1= H*PY(2)
                  YT(1)= Y(1)+RK1*.5D0
                  YT(2)= Y(2)+RL1*.5D0
                  Z= Z+HH
                  CALL FCNI(Z,YT,PY,K)
                  RK2= H*PY(1)
                  RL2= H*PY(2)
                  YT(1)=Y(1)+RK2*.5D0
                  YT(2)= Y(2) +RL2*.5D0
                  CALL FCNI(Z,YT,PY,K)
                  RK3= H*PY(1)
                  RL3= H*PY(2)
                  YT(1)= Y(1) +RK3
                  YT(2)= Y(2)+RL3
                  Z= Z+HH
                  CALL FCNI(Z,YT,PY,K)
                  RK4= H*PY(1)
                  RL4= H*PY(2)
                  Y(1)= Y(1)+(RK1+RK4+2*(RK2+RK3))/6
                  Y(2)= Y(2)+(RL1+RL4+2*(RL2+RL3))/6
                  IF (Y(1) .GT. 1) GO TO 10
                  IF (Y(1) .LT. TA) GO TO 11
             500  CONTINUE
             780  CONTINUE
                  RETURN
              10  CONTINUE
                  IF (IFLAG .EQ. 0)
                 1WRITE(6,1000) Z,Y
                  IFLAG= 1
                  RETURN
              11  CONTINUE
                  IF (IFLAG .EQ. 0)
                 1WRITE(6,1000) Z,Y
                  IFLAG= -1
                  RETURN
            1001  FORMAT(10I8)
            1000  FORMAT(8E15.8)
                  END

@HDG   RIBBON FCNI  .L,1
```

FEB 7 1982

FLAT PLATE SOLAR ARRAY PROJECT

Contractor Quarterly, Annual, Interim, and Final Report Distribution List

Distribution List #645 - Device Measurements and Research Task
(Total = 140 Copies)

	No. of copies
Applied Solar Energy Corporation Attn: D. C. Leung 15251 East Don Julian Road City of Industry, CA 91746	1
Arco Solar, Inc. Attn: Library/Aggie Raeder 20554 Plummer Street Chatsworth, CA 91311	1
Arco Solar, Inc. Attn: H. I. Yoo 20554 Plummer St. Chatsworth, CA 91311	1
Arizona State University College of Engineering Science Attn: Dr. Charles E. Backus Tempe, AZ 85281	1
Battelle Memorial Institute Columbus Laboratory Attn: Dr. Donald C. Carmichael 505 King Avenue Columbus, OH 43201	1
BDM Corporation Attn: Mr. J. Scott Hauger 7915 Jones Branch Drive McLean, VA 22101	1
Bell Aerospace Textron Attn: Mr. Frank M. Anthony P. O. Box 1 Buffalo, NY 14240	1
Boston College Attn: Dr. P. H. Fang Dept. of Physics Chestnut Hill, MA 02167	1
Brown University Department of Engineering Attn: Dr. Joseph J. Loferski Providence, RI 02912	1

	No. of Copies
Central Solar Energy Research Corp. Attn: Dr. W. Lance Haworth, PH. D. 328 Executive Plaza 1200 Sixth Street Detroit, MI 48226	1
Comsat General Corp. Attn: Denis Curtin 950 L'Enfant Plaza, SW Washington, DC 20024	1
Cornell University College of Engineering Dept. of Material, Science & Engr. Attn: Dieter G. Ast Ithaca, NY 14850	1
Crystal Systems, Inc Attn: Frederick Schmid Shetland Industrial Park 35 Congress St. Salem, MA 01970	1
Dow Corning Corporation Solid State Research Attn: Dr. L. D. Crossman Mail #092 Midland, MI 48640	1
Dow Corning Corporation Attn: Vishu Dosaj 12334 Geddes Road Hemlock, MI 48626	1
Eaton Corporation Semiconductor Equip. Oper. Nova Implantation Systems Attn: Allen R. Kirkpatrick 16 Tozer Road Beverly, MA 01915	1
Electric Power Research Institute Attn: E. A. De Meo 3412 Hillview Avenue P. O. Box 10412 Palo Alto, CA 94304	1

	No. of copies
Electric Power Research Institute Attn: Frank R. Goodman 3412 Hillview Avenue P. O. Box 10412 Palo Alto, CA 94304	1
Energy Materials Corporation Attn: Dave Jewett Ayer Road Harvard, MA 01451	1
Exxon Research & Engineering Co. Attn: Dr. James Amick P. O. Box 8 Linden, NJ 07036	1
General Electric Company Attn: R. N. Hall Corp. R & D P. O. Box 43 Schenectady, NY 12301	1
GHS Consulting Attn: Dr. G. H. Schwuttke 6 Spur Way Ponghkeepsie, NY 12603	1
Honeywell, Inc. Corporate Technology Center Attn: J. D. Heaps 10701 Lyndale Avenue South Bloomington, MN 55420	1
Jet Propulsion Laboratory Attn: (Contract Negotiator) M/S 511-303 4800 Oak Grove Drive Pasadena, CA 91109	1
Jet Propulsion Laboratory Attn: Solar Data Center M/S 502-414 4800 Oak Grove Drive Pasadena, CA 91109	35
Jet Propuslion Laboratory Technology Utilization Attn: L. P. Speck M/S 180-302 4800 Oak Grove Drive Pasadena, CA 91109	1
Kayex Corporation Hamco Division Attn: R. L. Lane 1000 Millstead Way Rochester, NY 14624	1
Kulicke & Soffa Industries, Inc. Attn: Max Bycer 507 Prudential Road Horsham, PA 19044	1
Lamar University Attn: Dr. Carl L. Yaws P. O. Box 10053 Beaumont, TX 77710	1
Arthur D. Little, Inc. Attn: Dr. David Almgren Room 20-531 Acorn Park Cambridge, MA 02140	1
Massachusetts Institute of Tech. Lincoln Laboratory Attn: Mr. Marvin Pope Room I-210 244 Wood Street or (P. O. Box 73) Lexington, MA 02173	1
Dr. H. F. Matare P. O. Box 49177 Los Angeles, CA 90049	1
Materials Research, Inc. Attn: Dr. Ram Natesh 790 East 700 South Centerville, UT 84014	1
Mobil Tyco Solar Energy Corp. Attn: K. V. Ravi 16 Hickory Drive Waltham, MA 02154	1
Mobil Tyco Solar Energy Corp. Attn: Fritz Wald 16 Hickory Drive Waltham, MA 02154	1
Monegon, Ltd. Attn: Scott Kaufman 4 Professional Drive Suite 130 Gaithersburg, MD 20760	1

	No. of copies
Monsanto Research Corporation Attn: H. Gutsche P. O. Box 8 St. Peters, MO 63376	1
Motorola, Inc. Semiconductor Group Attn: R. Gurtler 5005 East McDowell Road Phoenix, AZ 85008	1
Motorola, Inc. Semiconductor Group Attn: I. Arnold Lesk A-110 5005 East McDowell Road Phoenix, AZ 85008	1
NASA Headquarters Solar Terr. Systems Div. Attn: John Loria 600 Independence Ave., SW Washington, DC 20546	1
NASA Headquarters Attn: J. P. Mullin, Code RP-6 M/S B636 Washington, DC 20546	1
NASA Lewis Research Center Photovoltaic Project Office Attn: William Brainard M/S 49-5 21000 Brookpark Road Cleveland, OH 44135	5
NASA Lewis Research Center Attn: Dr. John C. Evans Jr. M/S 302-1 21000 Brookpark Road Cleveland, OH 44135	1
National Bureau of Standards Attn: Sam R. Coriell B164 Matls. Washington, DC 20234	1
National Bureau of Standards Attn: David E. Sawyer Bldg. 225, Room B-310 Washington, DC 20234	1
National Science Foundation Division of Applied Research Attn: Dr. Tapan Mukherjee 1800 G. Street N.W. Washington, DC 20550	1
Photon Power Attn: C. Lampkin 10767 Gateway West El Paso, TX 79935	1
RCA, Advanced Technology Labs. Attn: M. S. Crouthamel Building 10-8 Camden, NJ 08102	1
RCA, Laboratories David Sarnoff Research Center Attn: Arthur Firester Princeton, NJ 08540	1
Rockwell International Electronics Research Center Attn: Dr. R. P. Ruth D/540, HA32 3370 Miraloma Avenue Anaheim, CA 92803	2
Rockwell International Energy System Group Attn: Mr. B. L. McFarland Dept. 714 8900 Desoto Ave. Canoga Park, CA 91304	1
Bernd Ross Associates Attn: Dr. Bernd Ross 2154 Blackmore Court San Diego, CA 92109	1
C. T. Sah Associates Attn: Dr. C. T. Sah 403 Pond Ridge Lane Urbana, Il 61801	1
Semix Inc. Attn: Thomas Rosenfield 15809 Gaither Road Gaithersburg, MD 20760	1

	No. of copies
Silicon Technology Corporation Attn: Dr. George S. Kachajian P. O. Box 310 48 Spruce Street. Oakland, NJ 07436	1
Siltec Corporation Attn: R. E. Lorenzini 3717 Haven Avenue Menlo Park, CA 94025	1
Sol/Los, Inc. Attn: Milo Macha 2231 South Carmelina Avenue Los Angeles, CA 90064	1
Solamat, Inc. Attn: Dr. Barton Roessler 885 Watermann Ave. East Providence, RI 02914	1
Solar Energy Research Institute Attn: Dr. Charles J. Bishop 1617 Cole Blvd. Golden, CO 80401	1
Solar Energy Research Institute Attn: SEIC/LIBRARY 1617 Cole Blvd. Golden, CO 80401	1
Solar Energy Research Institute Attn: Gary Nuss 1617 Cole Blvd. Golden, CO 80401	1
Solar Energy Research Institute Photovoltaic Branch Attn: Ted Ciszek 1617 Cole Blvd. Golden, CO 80401	1
Solar Energy Research Institute Photovoltaic Program Office Attn: D. W. Ritchie 1617 Cole Blvd. Golden, CO 80401	1

	No. of copies
Solar Energy Research Institute Photovoltaic Program Office Attn: Dr. Tom Surek 1617 Cole Boulevard Golden, CO 80401	1
Solar Energy Research Institute Photovoltaic Program Office Attn: Dr. C. Edwin Witt 1617 Cole Blvd. Golden, CO 80401	1
Solar Energy Systems Attn: W. J. Kaszeta One Tralee Industrial Park Newark, DE 19711	1
Solar Power Corporation Attn: P. Caruso 20 Cabot Road Woburn, MA 01801	1
Solarex Corporation Attn: John V. Goldsmith 1335 Piccard Drive Rockville, MD 20850	1
Solarex Corporation Attn: Dr. Joseph Lindmayer 1335 Piccard Drive Rockville, MD 20850	1
Solec International, Inc. Attn: Ishaq Shahryar 12533 Chadron Avenue Hawthorne, CA 90250	1
Southern Methodist University Institute of Technology Electrical Engineering Dept. Attn: T. L. Chu Dallas, TX 75275	1
Spectrolab, Inc. Attn: Dr. J. Minahan 12500 Gladstone Avenue Sylmar, CA 91342	1

	No. of copies
Spectrolab, Inc. Attn: E. L. Ralph 12500 Gladstone Avenue Sylmar, CA 91342	1
Spire Corporation Patriots Park Attn: R. Little P. O. Box D Bedford, MA 01730	1
Stanford Research Institute Materials Research Center Attn: Dr. Angel Sanjurjo, G213 333 Ravenswood Avenue Menlo Park, CA 94025	1
Stanford University Center for Materials Research Attn: Dr. Robert S. Feigelson Stanford, CA 94305	1
State University of New York College of Engineering Department of Materials Science Attn: Dr. Franklin F. Y. Wang Stony Brook, NY 11794	1
Strategies Unlimited Attn: Dough Finch Suite 205 201 San Antonio Circle Mountain View, CA 94040	1
Texas Instruments, Inc. Semiconductor Group Attn: Dr. L. D. Dyer M/S 960 P. O. Box 225621 Dallas, TX 75265	1
Tideland Signal Corp. Attn: Mr. Carl Kotilla P. O. Box 52430 Houston, TX 770521	1
[illegible]W Systems Group Attn: Paul Goldsmith Bldg. M1/1334 One Space Park Redondo Beach, CA 90278	1
Underwriters Laboratories Attn: Al Levins 1285 Walt Whitman Road Melville Long Island, NY 11746	1
Underwriters Laboratories Attn: William J. Christian 333 Phingsten Northbrook, IL 60062	1
Union Carbide Corporation Attn: Mr. J. H. Lorenz 270 Park Ave. -8th Floor New York, NY 10017	1
Union Carbide Corporation Linde Division Attn: Dr. Hiroshi Morihara P. O. Box 44 Tonawanda, NY 14150	1
University of Delaware Dept. of Electrical Engr. Attn: Allen M. Barnett Newark, DE 19711	1
University of Illinois Materials Engineering Chicago Circle Compus Attn: Steven Danyluk Chicago, IL 60680	1
University of Pennsylvania Attn: Prof. Martin Wolf 308 Moore D2 Philadelphia, PA 19174	1
U. S. Airforce Air Force Aeropropulsion Lab. Attn: Mr. Joseph Wise AFAPL/POE-2 Wright-Patterson AFB, OH 45433	1
U. S. Army/MERADCOM Attn: DRDME-E/Mr. Donald D. Faehn Fort Belvoir, VA 22060	1
U. S. Department of Energy Forrestal Building Attn: Mr. Alan Postlehwaite 1000 Independence Ave., SW Washington, DC 20585	1

	No. of copies
U. S. Department of Energy Forrestal Building Attn: Dr. Morton Prince M/S 5G026 Photovoltaic Energy Systems 1000 Independence Ave., SW Washington, DC 20585	1
U. S. Department of Energy Technical Information Center Attn: Doc. Control & Eval. Branch P. O. Box 62 Oak Ridge, TN 37830	2 + Repro
Virginia Semiconductor, Inc. Attn: Dr. Thomas G. Digges, Jr. 1501 Powhatan St. Fredericksburg, VA 22401	1
Western Electric Semiconductor Materials Engineering Attn: R. E. Reusser - 6510 555 Union Boulevard Allentown, PA 18103	1
Westinghouse Electric Corporation Research Laboratories Attn: C. Duncan 1310 Beulah Road Pittsburgh, PA 15235	1
Westinghouse Electric Corporation Research Laboratories Attn: R. H. Hopkins 1310 Beulah Road Pittsburgh, PA 15235	1
Westinghouse Electric Corporation Advanced Energy Systems Division Attn: Dr. P. F. Pittman P. O. Box 10864 Pittsburgh, PA 15236	1
Westinghouse Electric Corporation Research Laboratories Attn: Dr. P. Rai-Choudhury 1310 Beulah Road Pittsburgh, PA 15235	1

	No. of copies
Westinghouse Electric Corporation Research Laboratories Attn: R. K. Riel 1310 Beulah Road Pittsburgh, PA 15235	1
Westinghouse Electric Corporation Research Laboratories Attn: Dr. R. G. Seidensticker 1310 Beulah Road Pittsburgh, PA 15235	1
Dr. Robert J. DeAngelis Dept. of Metallurgical Engineering University of Kentucky Lexington, KY 40506	